Thermic fluctuations of microtubules networks

Anders Rosengren

February 12, 2010

resume

En af cellens centrale komponenter er de lange hule cylindere bestående af tubulin-enheder, kendt som mikrotubuli. En af egenskaberne, hvorved disse karakteriseres er deres persistenslængde. Den er et udtryk for deres mekaniske fleksibilitet, og er derved særlig relevant, eftersom mikrotubli netop indgår i en længere række processer som bærende elementer. Denne rapport gennemgår tildels principperne bag en række eksperimenter fra litteraturen, hvori denne persistenslængde er bestemt. Tildels dokumenterer den desuden et fejlslagent forsøg i nærværende projekt på ligeledes at eksperimentelt bestemme denne, herunder fremkomsten af utilsigtede taxol krystaller.

Netværk af mikrotubuli polymeriseret med tilstedeværelsen af proteinet TPPP/p25 undersøges udfra mikro-rheologiske betragtninger vha. et optisk pincet setup. Dette afslører en diffusions eksponent $\alpha \approx 0.53$, der er lavere end den tidligere i litteraturen fundne $\alpha \approx 0.75$ for netværk af mikrotubuli dannet uden TPPP/p25.

Acknowledgements

The contents of present text aims to reflect work mainly done at the Niels Bohr Institute Optical Tweezers group 2008-2009. During this period a range of people has come to deserve the gratitude of the author.

My supervisor Ms. Lene Oddershede for accommodating me in the group, helping me throughout the project and for an extended display of patience.

The project was a continuation of the work of Mr. Istvan Horvath and he and his supervisors should be appropriately thanked for getting me started on the project and continued collaboration.

I wish to thank Ms. Svenja-Marei Kalisch for her time conducting polymerization experiments with me at the AMOLF institute in Amsterdam.

Lab-technician Ms. Inger Jensen, especially for services provided using the electron microscope.

The whole optical tweezer group for introducing me to their interesting scientific discoveries and through these enhancing my spirit, and for providing a pleasant work environment. This especially includes Mr. Shahid Aftab Mir for many hours in the lab and the discussion of many project related subjects.

Finally the whole B/C floor crowd, above persons included, for a pleasant social atmosphere and activities during and off work hours.

My parents and family.

Contents

Chapter 1

Preface

Microtubules are polymers consisting of tubulin subunits in a lattice formation curled into a hollow cylinder. They are key components of the cytoskeleton and are crucial in maintenance of cell shape, in several transport processes, in cell signalling and cell division. Microtubules are dynamic polymers and their assembly is tightly regulated both spatially and temporally. The functional diversity of microtubules is achieved through static and dynamic binding of various regulatory proteins. Descriptions of bio-polymers, such as microtubules, include continuously filament and ideal chain models. Mechanical properties such as their elastic moduli are key elements for understanding their function and abilities.

The Bending energy, or energy of deformation, of a microtubule in a ideal description as a thin rod in the Kratky-Porod model is given by:

$$E_{bend} = \frac{EI}{2} \int_0^l \left(\frac{d\mathbf{t}}{ds} \right)^2 ds, \tag{1.1}$$

$\mathbf{t}$ being the tangent vector, l the total length, s the arc length and EI the flexural rigidity- an object characteristic.

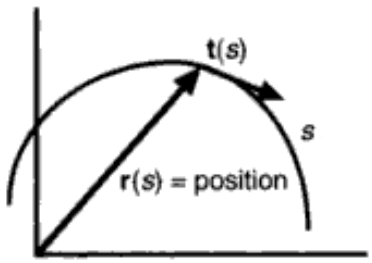

Figure 1.1: A bending thin rod coordinate-system

Since the discovery of microtubules a series of studies have reported their flexural rigidity with a large spread. Recently in 2006 a study [38] was done, suggesting the flexural rigidity to be length dependent. This is not in compliance with a traditional approach, where microtubules are thought of and modeled, as thin rigid rods or beams.

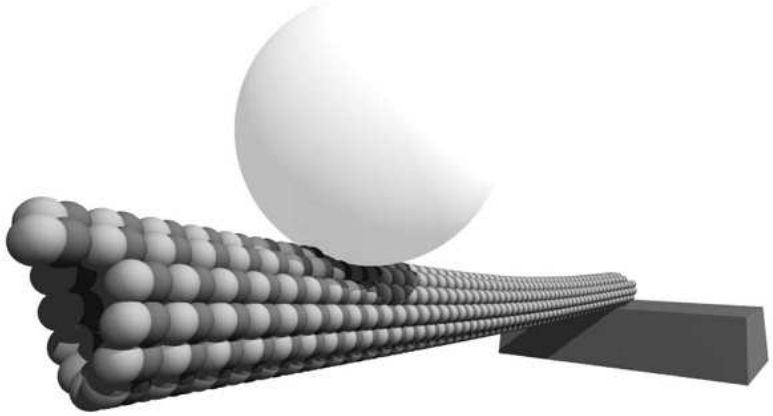

Figure 1.2: Schematic of a cantilevered microtubule with an attached polystyrene tracer bead. The bead was to be observed and manipulated through a optical tweezer setup.

The original aim of this project was to fixate one end of single microtubules on a gold grid and thereby making it a a cantilever, see figure 1.2. By attachment of tracer bead to the microtubule and observation of its movement, the flexural rigidity could have been determined, as the fluctuations of its shape due to energy exchange with the surroundings will obey to a Boltzmann distribution. An optical tweezer setup would provide both the position detection and a mean to manipulate the microtubule. Specifically it was hoped that the flexural rigidity of microtubules polymerized in presence of newly discovered microtubule associated protein TPPP/p25 could be determined, as this is currently undocumented. It was of equivalent interest to examine the proposed length dependency.

Unfortunately, the polymerization of single microtubules was never achieved and the experiment therefore was abandoned. Instead large networks of TPPP/p25 microtubules were examined by microrheology experiments. Microrheology is the observation of the movement of a embedded tracer particle. It is typically used to provide information of complex fluids such as gels or polymer solutions.

The present text reflects, that one line of experiments had to be abandoned and replaced by another of perhaps smaller yield. As a consequence,

it contains parts, that are somewhat more of a review-like than experimental nature, as also it seeks to present the process and the principles of the abandoned experiment.

Outline

Chapter 2 show the microtubules in biological context and on an introductory level tries to explain some the cellular processes in which they play a role. It then goes on to explain how the microtubule itself is constructed and the dynamic polymerization process behind it.

Chapter 3 treats the microtubule as an mechanical object and tries to highlight the major elements of the methods previously used to obtain the flexural rigidity. It also takes a closer look at the reported length dependence. It is sought to be done on a level of complexity true to the studies upon which it is based without going as vigorously into detail, as appropriate if the original experiments had been successful.

Chapter 4 Outlines some aspect of the original and abandoned experiment. It also introduces the networks of TPPP/p25 microtubules on which subsequent experiments were done.

In **chapter 5** Introduces the microrheology used to characterize the formed microtubule networks

Chapter 6 Introduces the optical tweezer setup and seeks to briefly explain the theory behind optical trapping. It also discloses the applied microscope technique differential interference microscopy.

Chapter 7 Reports and discusses the observations from the microtubules network polymerized in presence of TPPP/p25.

Chapter 8 Provides a short overall conclusion on the project.

In addition a small appendix consisting of a couple of protocols and at the end a very small glossary is provided mostly.

The reader be advised: A certain power exponent α as introduced in chapter 5, reappears under a number of terms including diffusion-, scaling-, power- exponent or coefficient, hopefully it will not be a cause of confusion.

Chapter 2

The cytoskeleton

A network of protein filaments is found in the cytoplasm of cells constituting the framework of the cell and it is accordingly termed the cytoskeleton. Both eucaryotes and procaryotes are found to have cytoskeletons but the composition and functionality displays a great variety in different cells. Cell shape, cellular motion and intracellular transport are among the processes which are facilitated through the cytoskeleton. These filaments are all made up of smaller units and in the end a smallest subunit can be identified; a protein or protein complex. The three major protein filaments of the animal cytoskeleton are, see figure 2.1:

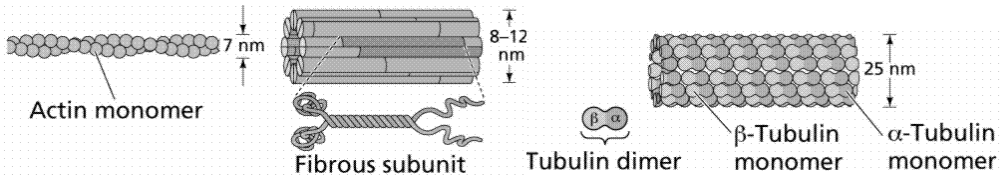

Figure 2.1: The three types of filaments of the cytoskeleton. *left* F-actin. *middle* Intermediate filament. *right* Microtubule. Figures from [52].

- **Actin filaments**: Also known as thin filaments or F-actin. The thinnest and least rigid of the filaments. It consists of two long helical intertwined polymers of G-actin (43 kDa). The diameter of the filament is $\approx 7nm$. Actin is one of the most abundant proteins in most cells, and is often concentrated just inside the cell perimeter, providing a connection between transmembrane and cellular proteins in addition to provide structural support. Actin will form dense networks effectively making local or extended areas completely viscoelastic, whereas

in other contexts only a few actin filaments are needed to fulfill a specific purpose. Actin filaments in conjunction with myosin drives the contraction in muscular cells, and ties the membrane between the two daughter cells at cytokinesis. It is also responsible for movement of cells that apply lamellipodia and microspikes, and the main constituent of microvilli.

- **Intermediate filaments**: The intermediate filaments is a common term for a list of different globular proteins that can form filaments, they are, however, all constructed in a similar manner. The chains of two non globular proteins interwinding in a helical manner makes up the fibreous unit that constitutes the basic building block of intermediate protofilaments. Two such fibreous units then forms a dimer (tetramer of the original protein) and then such eight protofilaments are arranged in a cylindrical configuration. The dimers may be both homo or hetereo and therefore the diversity of intermediate filaments is even larger than the number of proteins they consists of. The diameter of an intermediate filament is typically $10nm$ and their main purpose is to provide structural stability and resilience. Generally their mechanical properties are considered intermediate compared to the other two types although sparsely documented. Intermediate filaments include among others Desmin found in muscle cells connecting Z disks, and the many keratins, found in epithelial cells and tissues.

- **Microtubules**: The thickest, potentially longest and most rigid filament of the cytoskeleton. Typically thirteen protofilaments consisting of $\alpha-$ and β tubulin dimers of 110 kDa in longitudinal connection, forms the hollow cylindrical microtubule by lateral inter protofilament interaction. The outer diameter is approximately $25nm$, and the inner $15nm$. Tubulin is present in nearly all eucaryotic cells and is estimated to represent as much as 20% of the total protein content present in the vertebrate brain. This is mainly due to the large number of microtubules in the axons and dendrites of nervecells.

These filaments are the most remarkable "tools" for the cell when the mediation of mechanical stress and strain is needed. In the overall picture of a typical cell with distances in the micron range and forces in the piconewton range, actin and intermediate filaments have been described as ropes and microtubules as beams in analogy to the components of a building blueprint, due to their characteristics for handling tension and compression respectively. This is not generally a misleading picture, but must of course be evaluated for the specific process and circumstances of geometry, forces, numbers etc.

For instance an actin network, when dense enough, can withstand the typical pressure arising during cellular conditions.

Numerous other proteins present in the cell will crosslink, bundle and connect these filaments to their own kind, to the other types or to other parts of the cell such organelles and the membrane. Other proteins again will regulate their number, length and mechanical properties. The expression of the specific proteins of the filaments, regulated through DNA pathways, differs mostly between different types of cells rather than within the individual cell, and is hence not a regulatory parameter for the individual cells to adjust. The combination of the above provides the cell with a system versatile enough to handle the broad range of circumstances and processes where strains and stresses is needed. These include the ability to maintain or alter cell shape, arrange cell components and organelles within the cell, and movement of the cell itself (lamellipodia, flagella, cilia) or movement of substrates or other environmental objects (cilia, microvilli). In addition, and not of any minor importance, the cytoskeletal networks provides paths and orientation through the cell used for signal processes and transport of e.g. vesicles by motor proteins such as kinesins.

2.1 Microtubules

The roles of microtubules are many and the following is a short presentation of some of these. Microtubules consist of long rows of polymerized α and β tubulin dimers, each row termed a protofilament; these will through lateral connections form the hollow cylinders that are microtubules. The polymerization processes is described in more detail in a following section. For now it just stated that it is a dynamic process, where polymerization and depolymerization is constantly ongoing, changing not only the length of individual microtubules in real time but also making new microtubules as other disappear. One end is more actively growing and shrinking faster than the other. It has been termed the "plus end" while the other is "the minus end" accordingly. The lattice of the tubulin in microtubules is chiral with respect to the two designated ends, and it is therefore evident that microtubules are polar. It is this dynamic behavior and its regulation combined with mechanical properties and polarity which makes microtubules functional in a long range of cell processes and features.

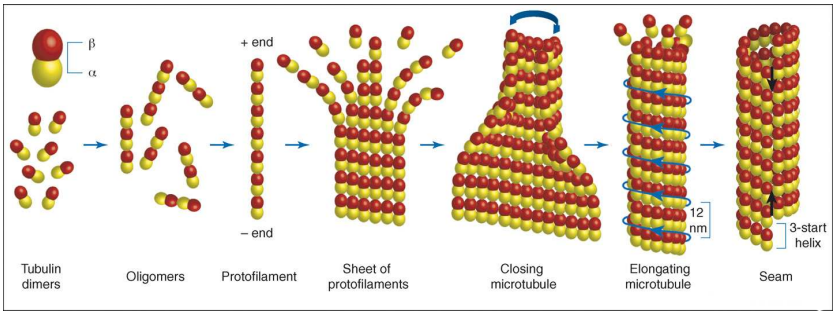

Figure 2.2: Polymerization of microtubules. A variation in the number of protofilaments gives different lattice structures compared to the one displayed for the most common type with 13 protofilaments, at the far right. Figure from [37].

Organizing centers

In most cells, microtubules are typically originating from one common center, where their minus ends are stabilized such that depolymerization is suspended. Such a center is called a microtubules organizing center and abbreviated MTOC, the most common MTOC's in animal cells are the centrosomes. They are located close to the cell nucleus.

The centrosome is a complex consisting of a pair of orthogonal centrioles placed within the centrosome matrix. Centrioles are a cylindrical arrangement of nine sets of fused microtubules triplets as seen in figure 2.3. Their diameter is approximately $200nm$ and their length the double. The centrosome matrix acts as a nucleation site for microtubules by unestablished mechanisms. A range of proteins are, however, known to be specific to the matrix including γ-tubulin which is thought to spontaneously form rings that will act as a platform for the further polymerization of $\alpha - \beta$ tubulin dimers into microtubules. At cell division the centrioles have duplicated and the centrosome divided into two. As the two centrosomes separate to opposite sides of the nucleus they form the two poles of the mitoticspindle.

At the base of cilium another MTOC is found, the basal body. It is essentially identical to a centriole, and formed by the duplication of a such. From the basal body a transition to another common microtubule pattern, known as the axonenemes appears. Axonemes form the base structure or scaffold of cillia and flagella. They consist of a central pair of single microtubules surrounded by nine doublet pairs. Cilia are best described as small hairlike extensions reaching out from the outer membrane of some cells. The movement of cillia either propels the cell or acts in conjunction with similar cells as small conveyor belts transporting various objects, such as eggs through the fallopian tubes and mucus up through the respiratory tract. Eu-

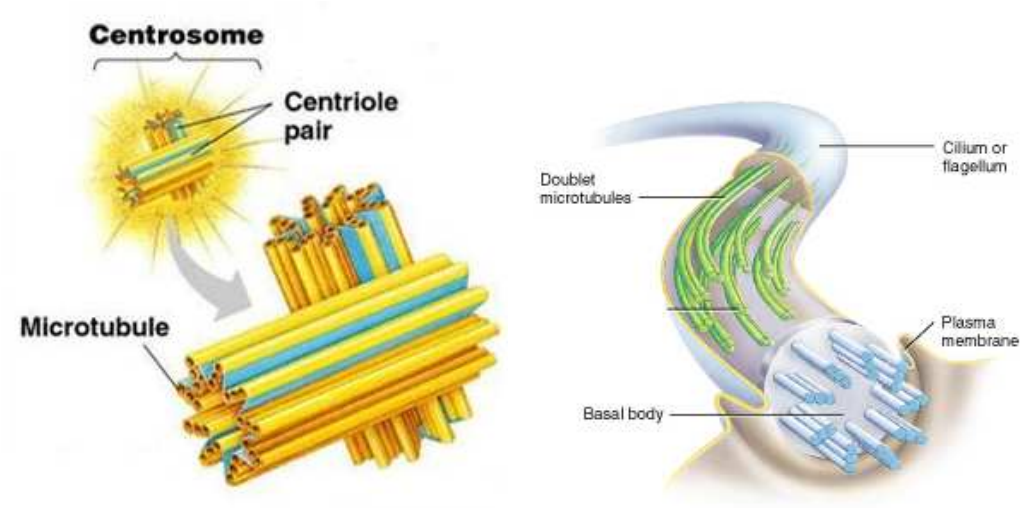

Figure 2.3: *Left:* The most common microtubule organizing centers of animal cells, the centrosomes. *Right:* The structure of a cilium or flagella. The basal body has the same buildup as a centriole. Figure from [5].

karyote flagella are similar to cilia except for being longer and more often appearing singulary; e.g they provide the propulsion of spermatocides. The microtubule associated motorprotein Dynein is responsible for the motion of cilia and flagella. As dyneins attached to one of the doublets starts to "walk" along an adjacent doublet it will introduce strain and ultimately result in the bending an consequently movement of the flagella. It should be noted that flagella of prokaryote move by a totally different mechanism.

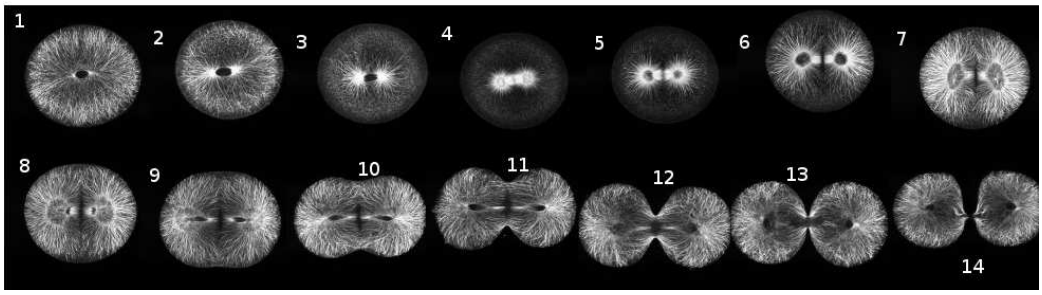

Figure 2.4: Confocal microscopy pictures of microtubule network during the elapse of mitosis of a Green Seaurchin Zygot. From the top left corner: 1: interphase, 2: incipient prophase, 3: prophase, 4: metaphase, $5-7$ anaphase, $8-10$: telophase, $11-14$: New interphase. Credits Victoria Foe.

As mentioned above, microtubules play a crucial role during mitosis of which an elaborate description is beyond this project. However, a brief

summary of the role of microtubules follows: At the onset of Mitosis, late prophase, the turnover rate of tubulin incorporated into microtubules dramatically increases from a microtubule halflife of approximatively 5 min to around 15 seconds. The existing microtubule network thus disintegrate and an abundance of new microtubules will start to grow from the centrosomes, as seen in 1-7 of figure 2.4. Exactly how this is accomplished is not fully understood but models include both proteins actively destroying microtubules and an increase in the number of nucleation sites in the centrosome matrix. The large number of new microtubules radiating out from the centrosomes, termed asters or astral microtubules, start to push the two centrosomes from each other to opposite sides of the nucleus. Overlapping regions of the microtubules from the two centrosomes will crosslink, such microtubules are called polar. This is the mitotic spindle, see figure 2.5

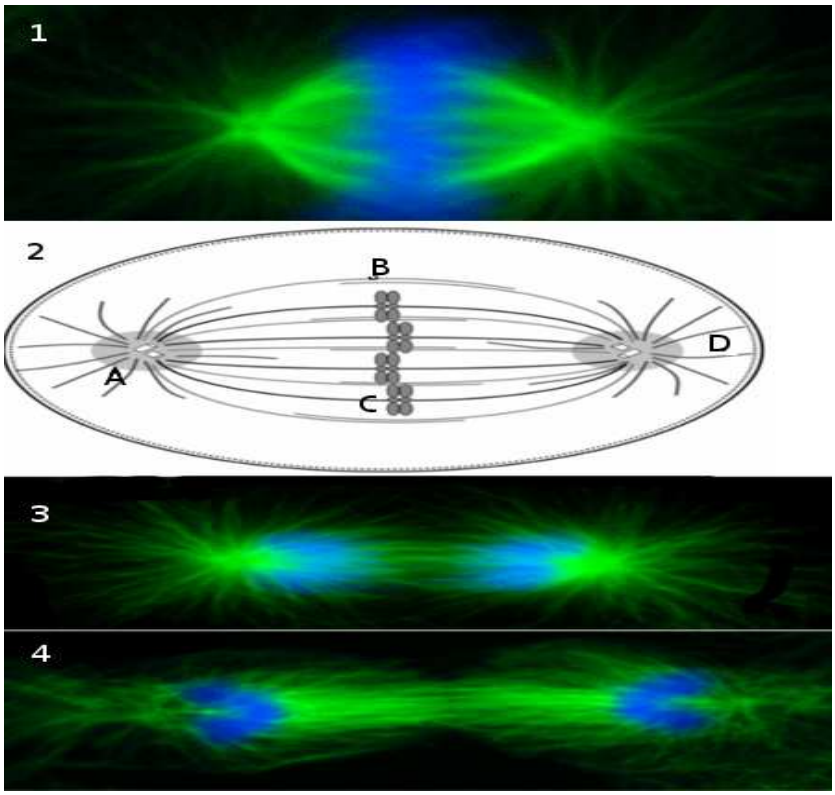

Figure 2.5: Confocal microscopy images of Xenopus XL-177 cells, credits Claire Walczak. Microtubules are stained green and chromosomes/DNA stained blue; 1: metaphase, 3: anaphase 4: telophase. 2: Schematic overview of the mitotic spindle at metaphase. 2A: The centrosomes, white cylindric centrioles. 2B: Polar microtubules, crosslinked by kinesin tetramers Eg5. 2C: Kinetochore microtubules attached to chromosomes. 2D: Astral microtubules which centers the centrosomes and explores the cytoplasm.

Other similar spindles exist for yeast and plant cell although having other MTOC's than centrosomes. As the nuclear envelope unfolds some of the newly forming asters will find and attach by the protein complexes kinetochores located at each chromatoid. For the microtubules that end up as polar or kinetochore microtubules normal dynamic behavior is suspended as they are stabilized.

When the inter-chromatoid connection in the chromosomes is broken, the mitotic spindle separates the chromatids by two methods, see figure 2.6. One is the sliding of the overlapping polar microtubules increasing the overall centrosome-centrosome distance. The other, shortening of the kinetochore microtubules. The sliding of polar microtubules is generated in their crosslinks by EG5-kinesins which also functions to arrange the mitotic spindle properly [47]. Kinesins are motor proteins that in general will walk toward the microtubule "plus end" fueled by the the hydrolysis of ATP. As the polar microtubules are antiparallel the motion of the kinesins will push them along making them slide past each other, see figure 2.6. The method by which the kinetochore microtubules shorten is not fully established. A once dominating model suggest the movement of the chromatoid towards the centrosome is mediated by motorproteins in the kinetichore and the subsequent depolymerization of the kinetichore microtubules. And indeed such "minus end" orientated proteins exist, the Dyneins, which are abundant at non microtubule bound kinetochores. However, in another theory it is the depolymerization and following structural change at the plus end that generates the movement. The dyneins in the later model are thought to serve a recruiting role for incoming astral microtubules as, in most animal cells, up to 20 microtubules are needed at each chromatoid before separation happens. Furthermore, the mechanisms for signalling "go" for the separation in anaphase to begin, and the avoidance of both chromatids binding to the same pole, seems to be connected to the tension of the kinetochore microtubules [32].

The function and role of the centrosomes and the mitotic spindle during mitosis as presented above was introduced by Kirschner and Mitchison in 1986 and is still accepted. Many aspects, however, remain unclear, e.g the above discussed mechanism of how the chromatids are reeled in. Other considerations regarding the mitotic spindle are the nucleation of microtubules at the kinetochore and subsequent orientation by tubulin concentration gradients [28] towards the centrosomes. Mechanisms as the later could perhaps help to explain the occurrence of mitotic spindles in cells deprived of their centrosomes. Also the reason for duplication of the centrioles and how the centrosome matrix functions are undisclosed at present. The answer might lie in the dynamic behavior of microtubules and its regulation mechanisms.

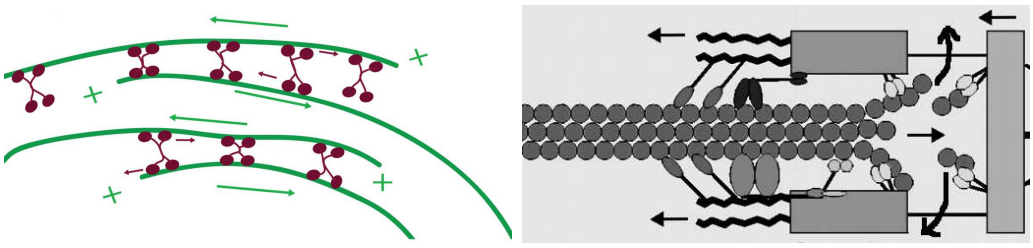

Figure 2.6: Separation of chromatoids *Left*: Increase of distance between the two centrosomes; Eg5 kinesin tetrameres will slide polar microtubules past each other as they walk. Figure from [47] *Right:* Shortening of kinetichore microtubules. Model of a microtubule (perfect circles) docked in a "sleeve" at the kinetichore complex, as the microtubule depolymerizes the kinetichore complex and thereby the chromatoid is made to move towards the left (microtubule minus end). Figure from [32].

2.2 Dynamics of microtubules assembly

The dynamics of microtubules is as mentioned based on the addition and loss of tubulin. Tubulin comes in five types α, β, γ, δ and ϵ. It is the α and β tubulin that form the dimers (length 8nm) that polymerize into microtubules. A large number of genes are known to transcribe tubulin and therefore it exists in a large number of subtypes, some specific to certain tissues and ascociated to specific conditions. The tubulin dimers of microtubules are arranged in strict pattern or lattice. Within the individual protofilament the dimers are always connected in an $-\alpha\beta - \alpha\beta - \alpha\beta$ sequence from minus to plus end, and neighboring protofilaments will be longitudinally displaced from each other by a certain amount. This is their chirality.

The polymerization of microtubules is accompanied by the hydrolysis of GTP. Both the α and β subunits of tubulin dimers bind GTP but only that of the β subunit will hydrolyze. This hydrolysation is thought to be the key element in the understanding of the dynamic behavior of microtubules.

Polymerization

In 1972 Weisenberg found the first examples of *in vitro* selfassembly of tubulin in solutions containing GTP. Since then it has been well establish that tubulin will self assemble in the presence of GTP and Mg^{2+}. In 1984 Mitchison and Kirschner proposed a behavior termed dynamic instability. The dynamic instability does not see the individual microtubules reaching a steady state length such as traditional polymerization theory and kinetics would predict, if feeded with certain tubulin concentration and number of nucleation cores. Instead it will switch between clearly distinguishable states of elongation/polymerization and depolymerization/shortning each of these pe-

riods described by their own kinetics. Dynamic instability as seen in Figure

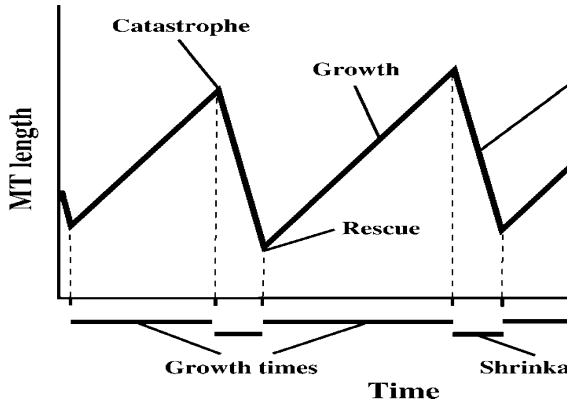

Figure 2.7: Dynamic instability. Figure from [24].

2.7 has since been established as the dominating mechanism of microtubule polymerization and observed directly in both *in vitro* and *in vivo* by methods such as DIC (differential interference contrast) microscopy. The rates of polymerization and depolymerization including association and dissociation constants, and the frequencies of catastrophes and rescues dependent on tubulin concentration was determined in the central paper [51] by Walker et al. in 1988 by direct observations of microtubules growing from an axoneme. See their original findings in Figure 2.8. In this paper similar dynamic instability was observed for both ends of microtubules which may seem somewhat surprisingly, given their rather different structure and association and dissociation rates. Even though dynamic instability of the minus end is of less or non physiological importance due to their arrangement in MTOC's, it provides additional information and constraints for models seeking to explain dynamic instability, which must incorporate this.

The findings of Walker et al. during elongation as seen in Figure 2.8 top left is described by following equations. v the rate, k_2 association and k_{-1} dissociation constants and $[T]$ the concentration of free tubulin:

$$v^{e+} = \frac{dn^+}{dt} = k_2^{e+}[T] - k_{-1}^{e+} \tag{2.1}$$

$$v^{e-} = \frac{dn^-}{dt} = k_2^{e-}[T] - k_{-1}^{e-}, \tag{2.2}$$

where + and - refers to the filament end and ^{e} indicates elongation. It is clear that one can speak of a critical concentration $[T_c] = \frac{k_{-1}}{k_2}$ of free tubulin which must be exceeded for polymerization to be occurring at the specific

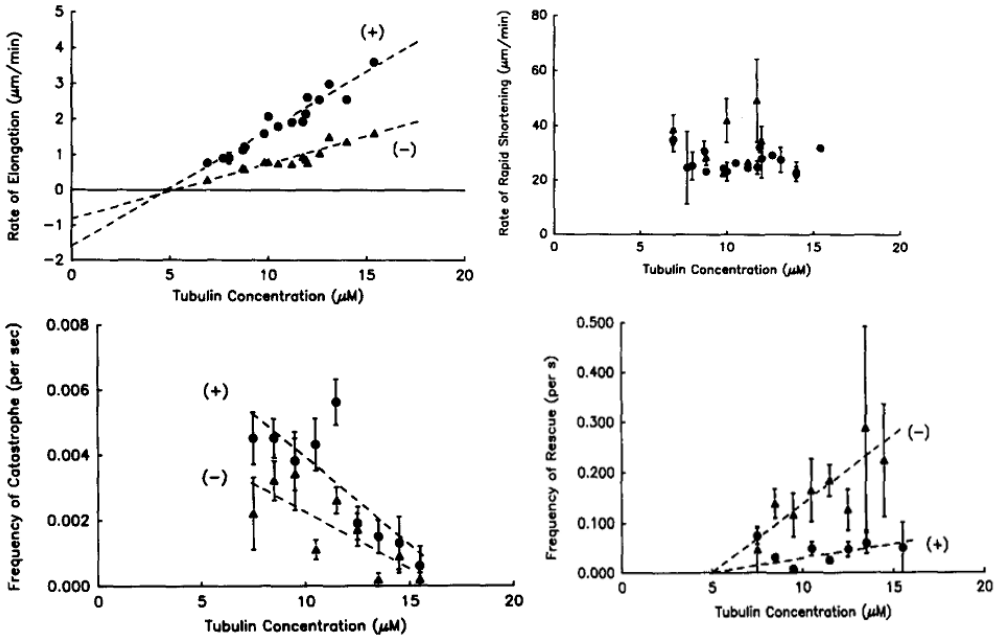

Figure 2.8: Dynamic instability. Original findings of Walker et al. 1988 [51]. Their findings qualitative and quantively are still the basis for characterization of dynamic instability.

end. Walker et al. found these two to be quite equal $4.9 \pm 1.6\ \mu M$ and $5.3 \pm 2.1\ \mu M$ for the plus and minus ends respectively. However, a scenario known as treadmilling at a intermediate concentration, where the net growth is zero due to one end polymerizing at same rate as the other depolymerizes is possible. Whether or not treadmilling occurs and is of any importance *in vivo* e.g as kinetochore microtubules wait for the connection of all chromosomes before separation or they simply are waiting statically due to stabilization is unknown.

The GTP cap model

As mentioned above tubulin will polymerize in the presence of Mg^{2+} and GTP, and the elongation periods are characterized by the addition of tubulin dimers bound to GTP, and the rapid disassembly periods by the release of GDP-tubulin. The hydrolysis of GTP, $GTP \rightleftharpoons GDP + P_i$, bound by tubulin happens very infrequently, but is enhanced considerably as the tubulin is incorporated into the microtubule lattice. Both the α and the β subunit binds GTP but only that of the β subunit will hydrolyze leaving it in a GDP bound state. Hydrolysis is not required for the assembly of tubulin, as

seen in experiments using non hydrolyzable GTP analogs such as GMPCPP. Such microtubules does not experience dynamic instability unless conditions are changed such that the GTP analogs are made hydrolyzable. These observations are the basis of the suggestion of a GTP cap as the mechanism responsible for dynamic instability.

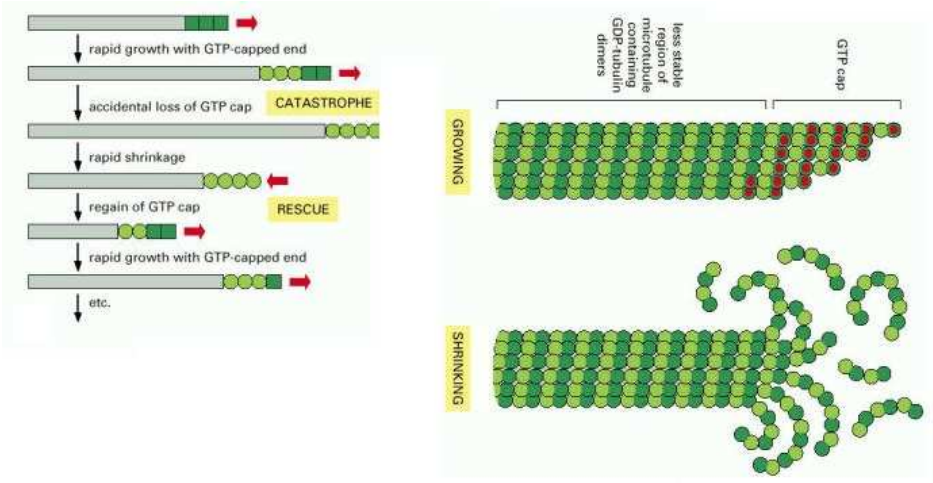

Figure 2.9: Schematic of the GTP cap model, where loss of the cap leads to a rapidly disassembling state. *left:* Squares and circles represents GTP and GDP bound tubulin subunits respectively. *right:* Here red dots represents unhydrolysed GTP of the subunits. Figures from [5].

The GTP cap model, see figure 2.9, postulates that the GTP hydrolysis leaves a core of GDP-tubulin within the microtubule, which is capped at the elongating end by a more stable region of GTP-tubulin subunits. Catastrophe is the loss of the GTP cap, and rescue is the recapping of a GDP-tubulin end during rapid shortening. Resent studies suggest and confirms that rescues to a greater extend should be be contributed to small pockets of un-hydrolyzed GTP-tubulin within the microtubule lattice rather than the reestablishing of a GTP cap by random addition of a GTP-tubulin dimer [12].

The orientation of $\alpha\beta$-dimers in the protofilaments as well as the tubulin lattice in a microtubules is as stated previously known. In the current GTP cap model hydrolysis of GTP of the β subunit will only occur as the unit is embedded in the microtubule lattice, meaning that the β-subunit needs residues from the α subunit of a incoming tubulin dimer as well as lateral connections to its neighbors to facilitate the hydrolysis of GTP. This means that in the case of hydrolysis being faster than tubulin addition, a single ring of GTP-tubulin at the microtubule end will be sufficient to keep it stable [6]. Whereas in the case where addition of new tubulin dimers is faster, the cap

will grow. Several experiments support the possible existence of such a small cap, and in some models depending on specific microtubule lattice structure as little as one GTP-tubulin is thought to be enough to stabilize the microtubule.

Since dynamic instability is clearly a non equilibrium process, and thus allows microtubules to perform work, it needs to somehow be powered. During periods of elongation it is the high affinity of GTP-tubulin that drives the polymerization, and it is substantial enough to overcome compressive forces in the piconewton range. The energy released by the hydrolysis of GTP causes a conformational change of the β tubulin subunit itself, or between the two subunits, $\alpha - \beta$, of the dimer, which is stored as stress in the microtubule lattice. This energy is what drives the rapid disassembly, and lets microtubules perform work as they shorten. The structural change has been observed as the polymerizing end of a free microtubule is most often seen to be a sheet of protofilaments, which closes into the cylindrical microtubule, but is complete different during disassembly, where the individual protofilaments are seen to curl up outwards as seen in figure 2.10 These horns of curling protofilaments at the disassembling end might be the mechanism of which some proteins identify microtubules ends.

The exact structural differences between GDP-tubulin, GTP-tubulin and $GDP + P_i$ -tubulin free and incorporated into the microtubule lattice are, however, not yet fully established, and thus neither the processes of the GTP cap and microtubule assembly and disassembly. The latest experiments and models lean towards a lattice model where free tubulin remains in a "bend" configuration independent on its state of GTP or GDP. And where it is then straightened upon incorporation in the microtubule lattice, in favor of the original allosteric model where free GTP-tubulin already is in a more straight, and thereby polymerization friendly, conformation. This is in agreement with both the sheet formation and the polymerization of non hydrolyzing GTP analogs.

Studies have been done on microtubules growing under longitudinal compression [23], and thereby growing at a lower rate. They have shown these microtubules to experience catastrophes at a lower frequency compared to normal microtubules growing without opposing force. These findings are not in accordance with the findings of Walker et al. [51]. Simulations in [50] suggests that this could be because microtubules growing under pressure would have a blunt rather than the normal long sheet closing into the microtubule cylinder. A blunt end will offer fewer opportunities to lose the GTP cap. That microtubules growing under compression are less frequent to depolymerize makes sense with respect to cells. Microtubules under pressure must

clearly be interacting with something and therefore might serve a purpose whereas it might be more appropriate to release the tubulin units of non stresses microtubules for construction of new microtubules.

The above has not considered a stepwise approach of microtubule polymerization, where tubulin dimers rather form a number of oligomers before these then incorporate into a growing microtubule; indeed this does not seem to be the case under the most simple *in vitro* conditions. It is, however, possible and to some extent proven that this is the case *in vivo* mediated by some microtubules associated proteins, such as XMAP215 [27].

The following figure 2.10 gives the current views on the aspects of the polymerization of microtubules. It should be clear from the above that the exact mechanism and nature of this and the dynamic instabilities are not yet fully understood 25 years after its discovery.

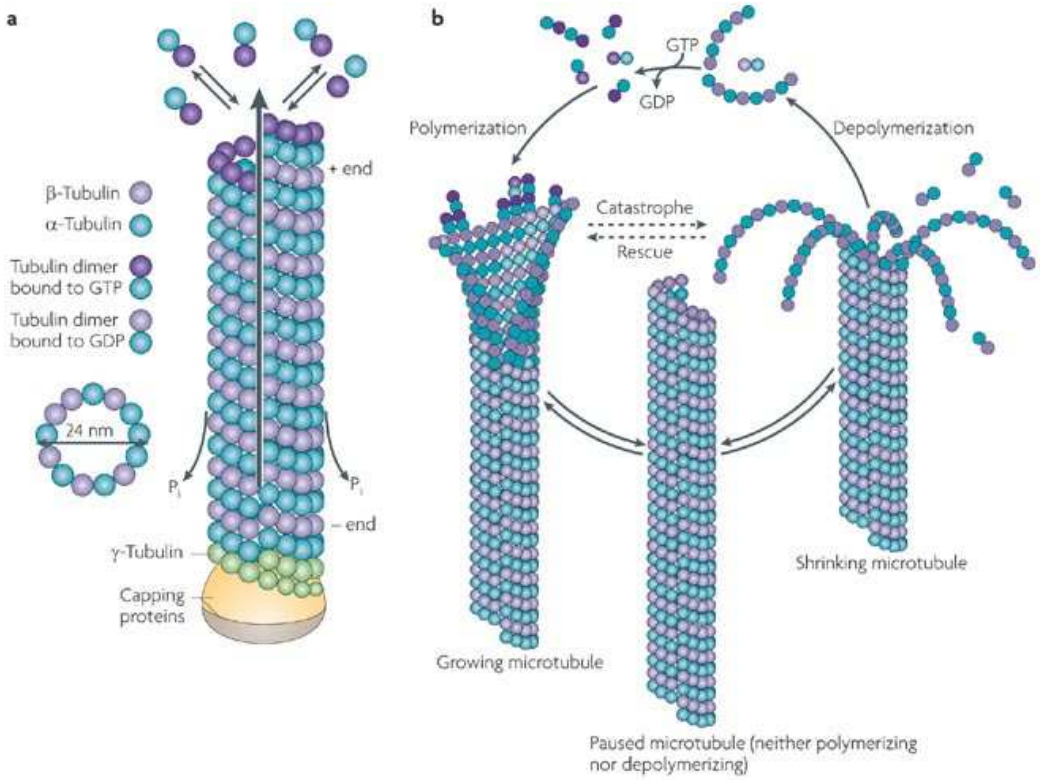

Figure 2.10: Polymerization of microtubules. Picture from [10]. Pauses occur very infrequent; already reported in 1988. The formed microtubules cylinders will consist of typically 13 protofilaments and have a outer diameter of approximately 25nm and and inner of approximately 15nm, and a length between 0.1-50microns.

Chapter 3

Flexural rigidity measurements

3.1 Microtubules as an simple beam

Microtubules function as mediators of strain and stress in the cell in a whole range of processes. In the following a quantification of mechanical properties is briefly introduced and followed by review of obtained values and the methods behind them.

If we look at a rod, it is intuitive that it will have some resting shape, and that if one wants to alter this shape, energy must be used. Such a bending energy E_{bend} would for a resting straight rod of length l bend into a uniform arc of radius R be:

$$E_{bend} = \frac{EI \cdot l}{2R^2}. \tag{3.1}$$

The quantity EI is termed the flexural rigidity and is specific for the object at hand as described below. The flexural rigidity is the most common parameter appearing in the literature and is strongly connected to engineering, however for biological systems and materials the persistence length L_p provides a more intuitive understanding of the polymers properties. Both quantities, which are straightforward related are used throughout this text. In equilibrium the shape of a rod or filament will alternate due to thermal fluctuations and as usual the likelihood of occupation for each state is distributed according to its energy and obeys a Boltzmanns distribution. The amplitude of these shape fluctuations can be quantified by the persistence length L_p

$$L_p = \frac{EI}{k_B T}, \tag{3.2}$$

where k_B is Boltzmanns constant and T the temperature.

If a microtubule is pictured as in figure 3.1 we introduce orthogonal coordinates, x along the unbent microtubule and y as the transverse deflection,

and the curve-linear coordinate s along the microtubule. The microtubule is hence described by coordinates $(x(s), y(s))$ or the tangent angle $\theta(s)$. and

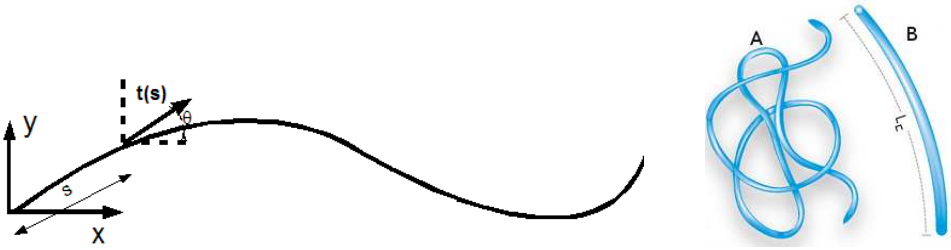

Figure 3.1: Schematic of microtubule shape, alongside the two limiting cases of length compared to persistence length; A: $l \gg L_p$, B: $l \ll L_p$. $\theta(s)$ is the deflection angle at point s along the curve. This coordinate-system is used throughout the following. Figure partially from [37].

we relate the persistence length to the correlation of tangential vectors $\mathbf{t}$ at the one end $\mathbf{t}(0)$ and along the filament $\mathbf{t}(s)$

$$\mathbf{t} = (cos(\theta), sin(\theta))$$

$$\langle \mathbf{t}(0) \cdot \mathbf{t}(s) \rangle = exp\left(-\frac{k_B T s}{EI}\right) = exp\left(-\frac{s}{L_p}\right) \tag{3.3}$$

If the total length is l we have two limiting cases:

$$l \gg L_p \Rightarrow \langle \mathbf{t}(0) \cdot \mathbf{t}(s) \rangle \approx 0$$

and

$$l \ll L_p \Rightarrow \langle \mathbf{t}(0) \cdot \mathbf{t}(s) \rangle \approx 1.$$

In the first case the filament appears wiggly, and in the later it resembles a rigid rod.

The general version of 3.1 with the above notation and parameters is called the Kratky-Porod model and given as:

$$E_{bend} = \frac{EI}{2} \int_0^l \left(\frac{d\mathbf{t}}{ds}\right)^2 ds \tag{3.4}$$

The following table 3.1 presents the values for the flexural rigidity of microtubules determined in different experiments from 1993-2009.

Taxol or Pacxilated(tm) is a small molecule found in the Pacific Yew tree and is the most common used stabilizing agent for microtubules essays. It stabilizes microtubules at substoichiometric concentrations as it binds to tubulin and prevents rapid disassembly and is apparently related to a enhancement

Table 3.1: Experimental persistence lengths determined from 1993-2009. Some of the experiments where also done in the presence of different MAP's, but values for such have been omitted from present table since these are, most often, only reported in single studies. Persistence lengths are all obtained *in vitro* and the presented values are for the majority calculated from flexural rigidity through equation 3.2. Where the temperature is given in an interval the persistence length has been calculated for $T = 25^oC$. See figure 3.2 for a brief overview of the methods.

	Method	EI $[10^{-24}Nm^2]$	L_p $[mm]$	T $[^oC]$	year ref.
Regular	Buckling force	7.9	1.9	33	2006 [29]
	Buckling force	6.8	1.7	25	1995 [45]
	Hydrodynamic flow	8.5	2.0	37	1994 [49]
	Hydrodynamic flow	35.8	8.4	37	1995 [30]
	Relaxation (RELAX)	3.7	.9	22-25	1996 [13]
	Relaxation (WIGGLE)	4.7	1.1	22-25	1996 [13]
	Thermal fluctuation	26.0	6.1	37	1995 [35]
	Thermal fluctuation	4.6	1.1	37	1994 [49]
	Thermal fluctuation	26.5	6.2	37	1995 [30]
	Thermal fluctuation	18.5	4.5	25	2001 [8]
	Thermal fluctuation	13.7-27.0	3.4-6.6	23	2004 [22]
	Thermal fluctuation	29.0	7.0	30	1997 [7]
Taxol stabilized	Buckling force	2.0	0.5	33	2006 [29]
	Buckling force	2.0	0.5	37	1995 [33]
	Buckling force	2.4	0.6	25	1995 [45]
	Buckling force	6.1	1.5	25	2009 [48]
	Relaxation (RELAX)	1.0	.2	22 25	1996 [13]
	Relaxation (WIGGLE)	1.9	0.5	22-25	1996 [13]
	Thermal fluctuation	21.5	5.2	25	2001 [8]
	Thermal fluctuation	32.0	7.5	37	1995 [35]
	Thermal fluctuation	2.4	0.6	37	1994 [49]

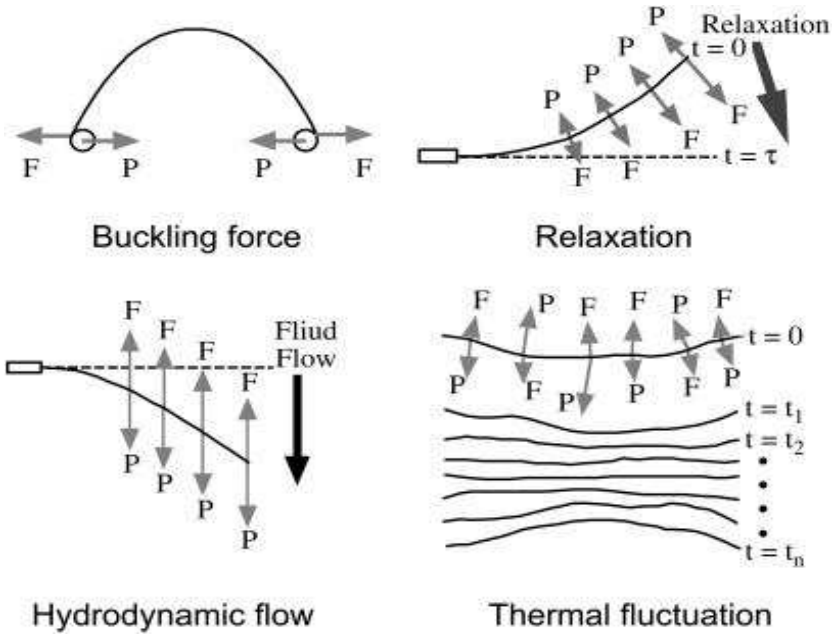

Figure 3.2: Methods used for determining the flexural rigidity of microtubules. P is the forced that is acting on the microtubules and F the internal force originating from the microtubules elastic response. Figure from [29]. In the static buckling force experiments the force is applied by optical tweezers and analysis based upon classical mechanics. Hydrodynamic flow experiments have the force originating from a fluid flow and hydrodynamics is the basis of analysis. In the dynamic relaxation/wiggle experiments the microtubules are moved by optical tweezers and analysis likewise based upon hydrodynamics. Thermal fluctuation experiments, where the microtubules shape is simply observed over time, are obviously an approach from statistical mechanics.

of microtubule flexibility. It is used as a treatment of lung, ovarian and breast cancer and other forms of cancer, as stabilized microtubules suspends mitosis of the cancer cells. Thus values of rigidity determined with taxol stabilized microtubules are not necessarily biologically relevant. The use of taxol in experiments may introduce further complications, as explained later. It is clear that the values have quite some variation, and that there unfortunately does not even to seem be a good correlation within the used method. Several of the values are in addition based upon a very little number of microtubules $N < 10$. Before further discussion, the following sections will illustrate the principles behind the methods to determine the persistence lengths, and outline how they are used in practise. The sections only tries to establish the basics of each method and tries to avoid cluttering by application of too many specific setup conditions and boundary conditions.

Common and very central for the methods is that microtubules are idealized as an isotropic homogenous continuously thin rigid rod or beam, such

that the beam equation relating force and curvature apply:

$$EI\frac{d\theta}{ds} = M, \tag{3.5}$$

where we introduce the bending moment or torque M. By expressing the curvature $\frac{1}{R} = \frac{d\theta}{ds}$ by deflection y: $\frac{d\theta}{ds} \approx \frac{d^2y}{dx^2}$, as reasonable for a small bending, and introducing the load per unit length, $w = \frac{dP}{dx}$ and realizing the relation $\frac{d^2M}{ds^2} = w$. We arrive at the Euler-Bernoulli beam equation:

$$\frac{d^2}{ds^2}\left(EI\frac{d^2y}{ds^2}\right) = w \Rightarrow EI\frac{d^4y}{ds^4} = w. \tag{3.6}$$

the last step assumes that the flexural rigidity EI does not vary along the beam. It is a functional differentiation of the kratky-Porod model of equation 3.4. The flexural rigidity EI can for isotropic materials be divided into a elastic constant Youngs modulus E, bigger means stiffer, and I the moment of inertia of the cross section, or more explicitly, the area weighted integral of the squared distance from an axis. For a hollow cylinder, such as a microtubule, of outer radius $x = R$ and inner $x = r$ I is given as:

$$\begin{aligned} I &= \int x^2 dA = \int_0^R x^2\left(R^2 - x^2\right)^{\frac{1}{2}} dx - \int_0^r x^2\left(R^2 - x^2\right)^{\frac{1}{2}} dx \\ &= \int_0^R \int_0^{2\pi} r d\phi r^2 cos^2\phi - \int_0^r \int_0^{2\pi} r d\phi r^2 cos^2\phi = \frac{\pi}{4}\left(R^4 - r^4\right). \end{aligned} \tag{3.7}$$

A microtubule have an inner radius of approximately 15nm and an outer 25nm.

Please review figure 3.2 beside the following explanations.

Buckling force

Buckling force experiments are based upon the introduced beam theory and observations of the bending of a microtubule subjected to forces. Observation are done directly by microscopy and forces most often applied by the use of an optical trap; experiments include [29], [33] and [45].

Traditionally such bending of beams under pressure would be evaluated with respect to the critical compression force, originally determined by Euler, needed for a straight beam to buckle assuming the ends are free to rotate:

$$P_{buckle} = \pi^2\frac{EI}{l^2} \tag{3.8}$$

However, since the exact onset of bending is very hard to experimentally determine, a range of geometric values together with the force can advantageously be observed instead.

Strictly speaking we already here abandon the equations above as the derivation in the following in principle does not require an assumption of an small deflection, in fact equation 3.10 is the exact beam equation.

Let subscript "0" refer to an initial state/shape of a microtubule of length l_0 which then is deformed into a new state by the application of force P as in figure 3.3. The force generates a bending moment which together with the

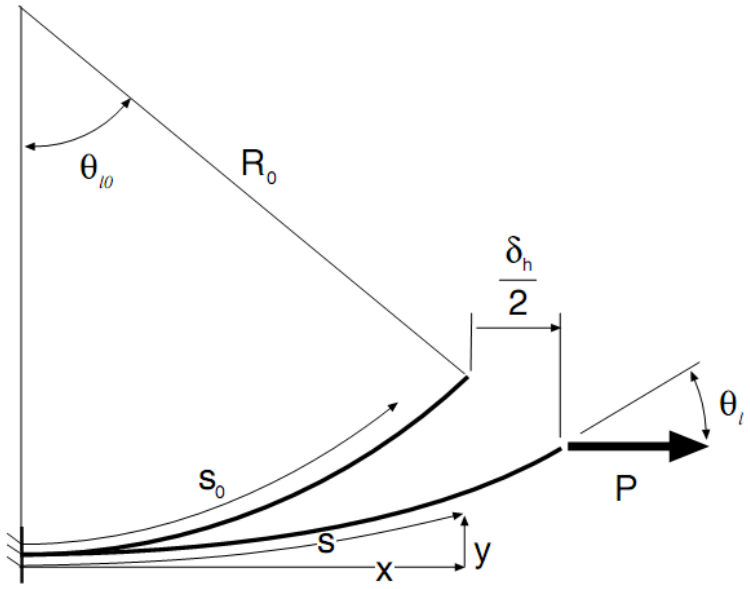

Figure 3.3: Schematic of 'half' a rigid rod, it is symmetric in respect to the vertical line. The end coordinate translate from $(x_0, y_0) \rightarrow (x + \frac{\delta x}{2}, y_0 - \delta y) = (x, y)$

original curvature gives the new curvature:

$$\frac{d\theta}{ds} = \frac{M(x)}{EI} + \frac{1}{R_0} = \frac{1}{R_0} - \frac{P(y(l) - y(s))}{EI}, \tag{3.9}$$

where we have used equation 3.5 and written the bending moment as $M = P(y(l) - y(s))$, the minus sign is due to the curvature becoming less when applying force as in the figure. If we differentiate and include $\frac{dy}{ds} = sin\theta$:

$$\frac{d^2\theta}{ds^2} = \frac{P}{EI} sin(\theta), \tag{3.10}$$

and then integrate this differential equation by first multiplying with $2\frac{d\theta}{ds}$ and making uses of the identity: $\frac{d}{ds}\left(\frac{d\theta}{ds}\right)^2 = 2\frac{d\theta}{ds}\frac{d^2\theta}{ds^2}$ we end up with:

$$\left(\frac{d\theta}{ds}\right)^2 = -2\frac{P}{EI}cos(\theta) + K, \tag{3.11}$$

K is a integration constant. Now we can express the curvature as:

$$\frac{d\theta}{ds} = \sqrt{\frac{1}{R_0^2} - \frac{2P}{EI}(cos(\theta) - cos(\theta_l))}, \tag{3.12}$$

θ_l is the deflection angle of the end position and the x-coordinate must be:

$$x(l) = \int_0^l cos\theta ds = \int_0^{\theta_l} \frac{cos(\theta)}{\sqrt{\frac{1}{R_0^2} - \frac{2P}{EI}(cos(\theta) - cos(\theta_l))}}. \tag{3.13}$$

The above equation have solutions of incomplete ecliptic integrals of the first $E_1[V|n]$ and second kind $E_2[V|n]$, which can be looked up in a table.

$$x(l) = m\sqrt{\frac{EI}{P}}\left(\left(1 + \frac{2}{m^2}\right)E_1\left[\frac{\theta_l}{2}|-m^2\right] - \frac{2}{m^2}E_2\left[\frac{\theta_l}{2}|-m^2\right]\right) \tag{3.14}$$

$$m^2 = \frac{4PR_0^2}{EI - 4PR_0^2 sin^2(\frac{\theta_l}{2})}. \tag{3.15}$$

Finally we can now find the displacement which must be given by:

$$\delta_h = 2x(l) - 2x_0(l_0) = 2x(l) - 2R_0 sin(\theta_{l0}), \tag{3.16}$$

and thus a function of the initial curvature $\frac{1}{R_0}$, the flexural rigidity EI and force P. The augment $V = \theta_l$ for the ecliptic integrals depends on whether or not the rod extends/compress. Microtubules are modeled as incompressible and thus maintains the same length:

$$l = l_0 = \int_0^l ds = \int_0^{\theta_l} \frac{d\theta}{\sqrt{\frac{1}{R_0^2} - \frac{2P}{EI}(cos(\theta) - cos(\theta_l))}}, \tag{3.17}$$

which also is solved by ecliptic integral of the first kind

$$l_0 = m\sqrt{\frac{EI}{P}}E_1\left[\frac{\theta_l}{2}|-m^2\right]. \tag{3.18}$$

Numerical solutions can determine the end angle θ_l with respect to P and hence allow for computation of the horizontal displacement according to 3.16 with insert of 3.14.

Now this may perhaps seem as quite some algebra, but the displacement and force are by far the easiest obtainable parameters in an optical tweezer experiment. Where one end of the microtubule is fixated while the other is moved closer by a optical trap, at a constant force. As the end is moved the microtubule will bend, building elastic energy, until the moving end suddenly escapes the trap. This provides an nicely definable event, such that the displacement and corresponding force can be acquired. Unfortunately, optical traps cannot trap a microtubule end, in fact it can be shown that the movement of the trap along a microtubule does not require energy, so handles are attached at the microtubule ends i.e. polystyrene beads. Since the force is not applied precisely at the ends due to these handles, see figure 3.4, it complicates the above derivation somewhat, as this gives rise to an "additional" bending moment at the microtubule ends. The overall equations thus becomes nonlinear [29]:

$$EI\frac{d\theta}{ds}_{s=0} = -Pcos(\theta(0)) \ , \quad EI\frac{d\theta}{ds}_{s=l} = -Pcos(\theta(l))$$

and is solved in a iterate numerical solution process, with the first estimate of EI value based upon the above equations 3.14-3.18. This first estimate is generally very close to the the final value. Now in most experiments the mi-

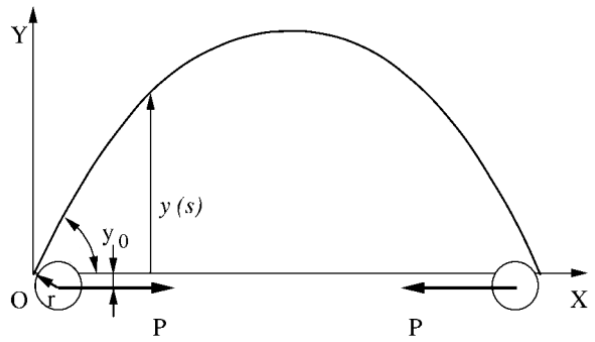

Figure 3.4: The applied force P must be mediated by the use of handles in experiments. Experiments are done by trapping each bead in a optical trap and then moving them closer untill one of the beads escape its trap, and the displacement/distance between the beads and the trapping force is obtained. Figure from [29].

crotubules original state will be a straight configuration. This however only slightly simplify the above derivations, which on the other hand, handles intrinsic curvature and accounts for bending both when pulling or pushing the

ends and allow for large angle deflections.

Relaxation and hydrodynamic flow

These kind of experiments are based on hydrodynamics where the load w of equation 3.6 is from the hydrodynamic force:

$$EI\frac{\partial^4 y}{\partial s^4} = -\gamma\frac{\partial y}{\partial t}. \tag{3.19}$$

γ is the perpendicular drag coefficient per unit length.

For the flow experiments one end $s = 0$ is fixated and the above equation solved in respect to a maximum deflection of the other end $y_{s=l}$, using a constant force density along the microtubule corresponding to a flow of constant velocity as in figure 3.2.

In the relax method; one end is likewise fixated and the other microtubule end deflected $y(t = 0)_{s=l}$ and then released. Corresponding values of time and deflection is then recorded $y(t)_{s=l}$. Since the the free end moves faster than the fixed end of zero velocity, a linearly velocity distribution between the ends is assumed. Ignoring inertial terms (assuming low Reynolds number) the end deflection is a first order differential equation with an exponential solution:

$$\left(\frac{y(t)}{y(0)}\right)_{s=l} = exp\left(EI \cdot t\right), \tag{3.20}$$

and by appropriate fitting the flexural rigidity be subtracted. A dynamic variant, where the fixated microtubule end is moved back and forth continuously causing the microtubule to oscillate, is called wiggle.

Considerations on the validity of these experiments are mainly concerned with the approximation of the hydrodynamic force, as this has a well established estimate for cylinders, but is unknown for structures such as microtubules; who to some extent allow passage of fluid through them. Experiments of this type include [49], [30] and [13].

Thermal fluctuations

These are actually identical to the above experiments in terms of theory, however, there is no manipulation to achieve a high deflection as the microtubules are freely floating. The shape of the microtubule is then simply observed as it fluctuates due to thermal influence. The hydrodynamic equation 3.19 is

in these experiments solved by describing the shape of the microtubule as a superposition of fourier modes(bending modes):

$$\theta(s) = \sum_{n=0}^{\inf} \theta_n(s) = \sqrt{\frac{2}{l}} \sum_{n=0}^{\inf} a_n cos\left(\frac{n\pi s}{l}\right) \tag{3.21}$$

From the equipartition of thermal energy into all bending modes the amplitudes a_n will be given.

This will yield relaxations times τ approximated by:

$$\tau \approx \frac{\gamma}{EI}(\frac{l}{\pi(n+1/2)})^4 \tag{3.22}$$

$n = 1, 2, 3, ...$ In experiments the shape or superposition were either manually mapped and subsequently digitized or found by algorithms of image analysis to allow numerical solutions, see experiments [35], [49], [30], [8] and [22].

The large spread of microtubule rigidity as illustrated by table 3.1 have been tried to be explained by several considerations. These include dependence on growth velocity [22] and temperature [26] during polymerization. Some variation of the rigidity could be obtained in these experiments. Unfortunately, the findings does not support each other, when considering the kinetics of higher temperature speeding polymerization up, and individually the variations found are not large enough to explain the large spread. To which degree the large variation of different experiments, at least partially, can be explained by systematical errors or weaknesses of the different methods is not clear. A possible source of error could be that different polymerization protocols of the different experiments could lead to microtubules with different number of protofilaments i.e different diameter and lattice with according change of flexural rigidity through the moment of inertia and elastic moduli. Variations of these kinds due to their expected size, does not immediately provide a satisfactory explanation of the large spread. Speculations could be that the individual experiments fail to observe single and individual microtubules but instead observe bundled or double/tri- walled specimens, but this remains purely speculative.

3.2 Length-dependent persistence length?

In 2006 Pamploni et al. published a study with the goal of establishing the persistence length of microtubules [38] and Taute et al. did a followup in 2008 confirming and elaborating on their findings [42]. Their experiment

was based on single stabilized microtubules fixated at one end and a fluorescent polystyrene bead attached somewhere along the free part of the microtubule, see figure 3.5. The microtubules were polymerized from pig tubulin from which 10% was biotinylated and 10% tetramethylrhodamine-labeled, to allow for the binding of neutravidin coated fluorescent polystyrene beads and make the microtubule itself fluorescent, respectively. After an initial polymerization period, the formed microtubules was resuspended in buffer containing $20\mu M$ taxol for stabilization.

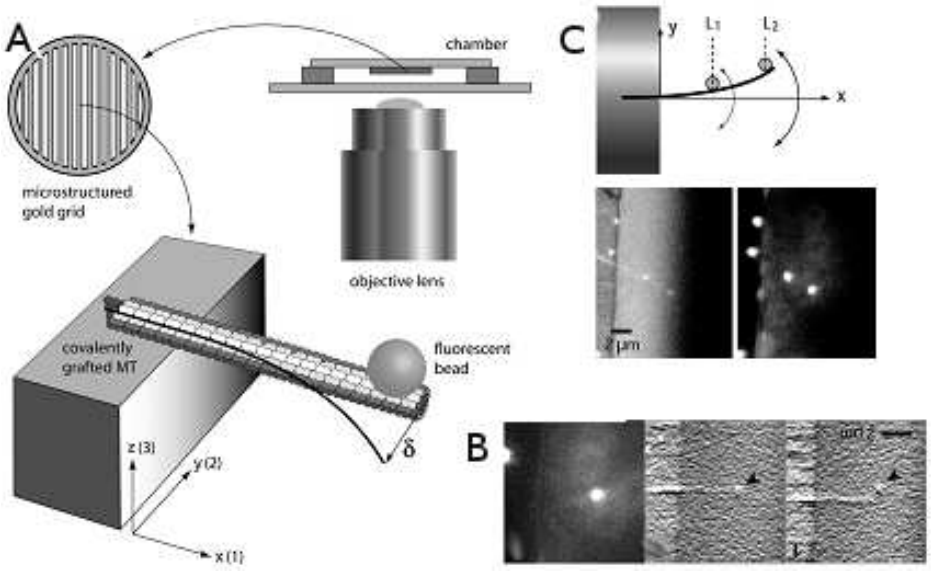

Figure 3.5: *A:* Schematic from the experimental setup of Pamploni et al. and Taute et al. *B:* 3 frames from the experiments. In the dark frames, a shadowing routine has been used to maximize contrast. *C:* To insure that found rigidity value was characteristic and not dependent on bead position, it was estimated independently by the movement of several beads at different positions for a number of microtubules. Figure is a mash up from [38].

The thermal fluctuations of the microtubule, i.e. the position of the fluorescent bead, was then determined by a single particle tracking algorithm from images acquired at a rate of 16 frames per second. The persistence length could then be found from the transverse distribution of the bead at:

$$L_P = \frac{L^3}{3\langle y(l)\rangle^2}. \tag{3.23}$$

The above equation can be derived from equations 3.5 with a point force acting at the end together with the small angle approach, and 3.4 and the equipartition theorem.

Pamploni et al. obtained values for 48 microtubules of varying length and surprisingly it revealed an increase of the persistence length up to 100-fold as a function of microtubule length, see figure 3.6. By determining and

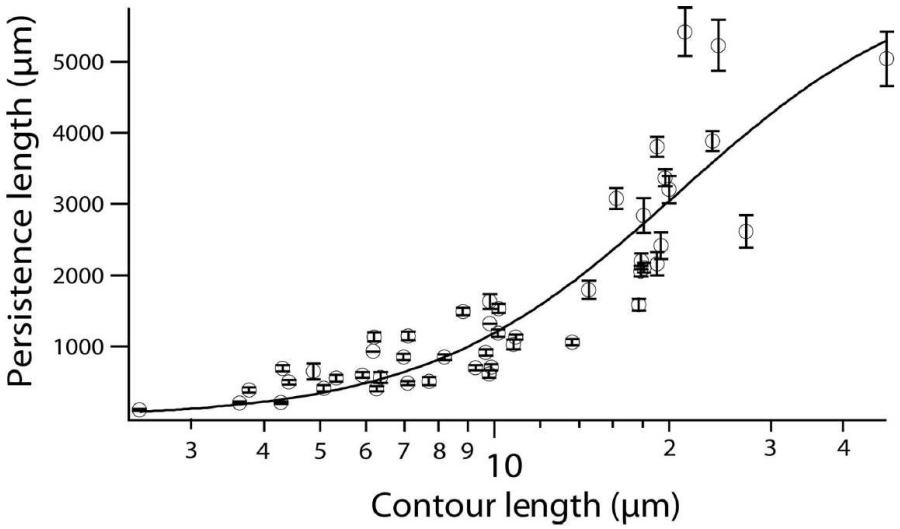

Figure 3.6: Original findings of length dependence of persistence length reported by Pamploni et. al. 2006 [38], the full line represents equation 3.25.

finding the same persistence length of the same microtubule, by attachment of beads at several positions along it, they concluded that the observation is that of the full microtubule length and not some position dependent phenomena. This is a surprising result as the persistence length as previously introduced is a characteristic based upon a material constant and geometry, and should be independent of length. Their conclusion was that it is too simplistic to review microtubules as isotropic rod, but instead should at least be considered as anisotropic with respect to the longitudinal dimension. A consequence must be that it is necessary to use the full tensors of stress and strain to deal with such a dimension dependent response to strain of microtubules. In the end they model microtubules as fiber reinforced materials that have a longitudinal anisotropy, but maintain a transverse isotropy and has relation between the longitudinal and transverse shear moduli. This directional dependency means that in terms of mechanical properties microtubules are better described more complex as a collection of filaments rather than a cylinder. Now we are already familiar with microtubules consisting of a smaller components i.e. the protofilaments. We can therefore formulate as the intra protofilament interactions of the tubulin subunits differs from the

inter protofilament interactions. It also means that microtubules of different protofilaments number and thereby alternative lattice structure very likely would give different material properties.

Keeping with this model, but using a different formalism than Pamploni et al. we regard microtubules as a number of crosslinked protofilaments and an understanding of the length dependence of persistence length can be outlined by relying on a few pointers from bundle mechanics. Each protofilament of a microtubule should be considered as an individual rod, but each of these protofilaments would interact with two neighboring protofilaments. The strength of this inter protofilament interaction must depend on their length since each tubulin subunit must contribute a fixed amount of binding energy.

From bundle mechanics it is known that if the coupling, i.e., the crosslinking of a bundle of filaments is weak, shear and shearing is allowed and that they therefore de facto act as independent filaments. If the coupling is strong, shear is not allowed and some filaments will have to stretch as others compress, for a bending of the bundle to be possible. The bending energy for such a bundle of semiflexible wormlike polymer chains, WLB, can be found by a composite hamiltonian:

$$H = H_{bend} + H_{stretch} + H_{shear}, \tag{3.24}$$

H_{bend} is the familiar one of equation 3.4 and represents the bending energy of each N filament, $H_{stretch}$ accounts for filament stretching/compression and H_{shear} for the energy of the crosslinks [17]. Bundles with weak coupling will have an persistence length proportional to the number of filaments while for strongly coupled bundles it will scale with the square of the filament number. The strength of the coupling must necessarily be related to the length of the filaments with some critical length separating weak from strong coupling.

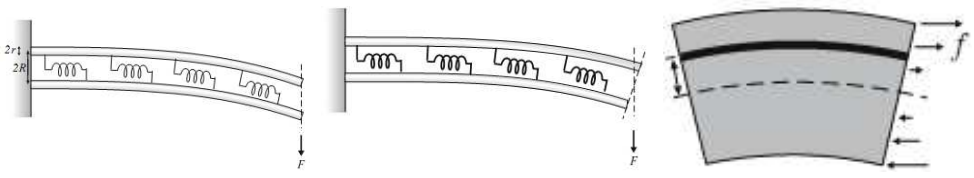

Figure 3.7: Bundles of N filaments. *left:* For weakly coupled elements the persistence length scales with their number, $L_p \propto N$. *middle* Strong coupled, persistence length scales with the number squared $L_p \propto N^2$. *right* In the case of strong coupling, a bundle behaves more like a single beam, and some elements will compress and other stress as the bundle is loaded. Figures from [19].

To recapitulate, bundle mechanics would predict one constant value for short microtubules and hence weakly coupled protofilaments and a larger value for long microtubules with strongly coupled protofilaments. Consequently for microtubules of intermediate length where a transition from weak to strong coupling of the protofilaments occur we should see increasing persistence length. In the first study of Pamploni et al., where there is an increase in rigidity, the following expression is derived to describe the increase of persistence length:

$$L_p(l) = \frac{L_p^\infty}{1 + (\frac{\lambda}{l})^2}, \tag{3.25}$$

where L_p^∞ is a constant persistence length of long microtubules and λ is introduced to account for protofilaments shearing. They fitted the data to this equation to obtain $L_p^\infty = 6.3mm \pm 0.8mm$ for "long" microtubules $l \gg \lambda \approx 21\mu m$; full line in figure 3.6. The degree to which the plot fits the data is not overwhelming as the fit does not include the majority of datapoints within the error bars given. Some spread of persistence length could be expected e.g if their number of protofilaments differ and subsequent have a difference in lattice/coupling, and may not be alarming by it self. It is perhaps more concerning that in regards to the shape of the curve, in reality and at best only one datapoint at $l \approx 47\mu m$ for "long" microtubules is present and there is large spread of the 3 next to longest microtubules.

Now from bundle mechanics it is also predicted that a constant persistence length must exist for short microtubules, and as a such is not apparent it was one of the goals of the followup by Taute et al, to establish. Taute et al. used the exact same setup as Pamploni et al. to obtain data of shorter microtubules. These findings can be seen in figure 3.8 please notice the interval of the axis! The full line is identical to equation to 3.25 with the values of the fit above, obtained earlier by Pamploni et al. They did not fit the new data to equation 3.25 due to a lack of a datapoint for a long microtubules. In this case the longest was approximately $30\mu m$ vs the one of the earlier study at $l \approx 47\mu m$. They conclude that the correlation of their data and the fit is evident for microtubules of length $l > 5\mu m$, whereas the values those shorter level to a plateu. They then continue to average the values of persistence lengths for the three shortest ones $L_p \approx 0.58 \pm 1mm$ to determine the value of this plateau, dashed line figure 3.8, and then establish it as the constant value predicted by bundle mechanics. To the author of present text their conclusion may not seem as evident as claimed.

A Length-dependent persistence length can, however, seem reasonable as it is not given, that a microtubule should be isotropic. We already stated

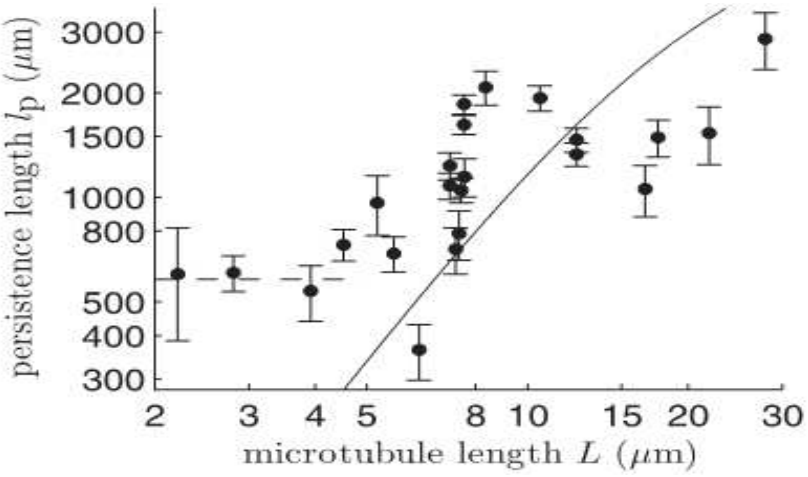

Figure 3.8: Reported values from the followup on length dependence of persistence length, by Taute et. al. 2008 [42] The dashed line indicates a constant value for the short microtubules, and the full line is equation 3.25 with the values obtained 2years prior by Pamploni et al.

that they consists of protofilaments and that their lattice will depend on the number of these protofilaments, and it would be strange should the binding energies of different lattices be identical. A such dependency could also provide the explanation for the large spread of the previously reported values of flexural rigidity. Intriguingly, if the above findings hold, the transition between a relatively low to a high persistence length occurs right around the typical length scale of cells, and therefore may be relevant in respect to the functionality of microtubules. Another consequence of viewing microtubules as bundles of protofilaments rather than single cylinders would be an upper length limit for axoneme based structures. As the length of the axoneme increases, so will the number of Dynein crosslinking the duplets, and although each dynein provides power a upper critical limit where the coupling becomes strong it will outpower the collected effort of the dyneins. Indeed an upper length for the axoneme tails of sperm seems to be existing estimated at approximately at $70\mu m$ and for a wide variety of species the tail length is always found to be lower [19].
A length dependent persistence length for microtubules was earlier speculated on by Tashiro et al. 1995 [33], but later dismissed in a followup [29]. Both were buckling experiments. It was also not seen by [26] by Kawaguchi et. al. earlier.

So even though a number of considerations would be in favor of length dependency it is perhaps not complete satisfactory established despite the efforts of Pamploni et al and Taute et al.

Our initial Motivation

The many different reported values of microtubule persistence lengths and the reported length dependence was an excellent subject for an experimental investigation. A setup similar to the one used by Pamploni et. al with a microtubule clamped in one end, as a cantilever, observed in an optical tweezer setup was desired to allow for one, several or all of the following:

- Estimations of the persistence length of a single microtubule based upon the above described methods: Buckling force, relaxation, wiggle, flow, thermal fluctuations. All possible to perform on the same microtubule in quick sequence, when done in a flowchamber on a piezo stage. Thereby in addition obtaining several estimates of the flexural rigidity for the same microtubules allowing for a comparison of the methods and a possible discovery of discrepancy.

- Finding the persistence length of four kinds of microtubules polymerized in the presence of one of the following: Taxol, GMPCPP, TPPP/p25 or GTP only.

- In addition by the use of electron microscopy if possible to resolve the protofilaments, to observe if the number would be different for the four kinds of microtubules or their polymerization protocol.

- Examine whether or not a length dependence of persistence length can be found for these types of microtubules and under which conditions.

Chapter 4

Experimental polymerization

4.1 Taxol, GMPCPP and trouble

The polymerization of tubulin into single microtubules should prove to be an impassable obstacle in achieving the original goals of this project. This is despite its apparent simplicity, and general consensus of available protocols. Their differences are mostly related to the purification of tubulin dating back to when it was not commercially available. A solution of water based general polymerization buffer or BRB80, $1mM$ GTP and tubulin in a concentration of no less than $1mg/mL \approx 10\mu M$ should self-assemble within a short time period into dynamic microtubules.

The reason for the unsuccessful polymerization remains unclear, the following was done:

- Care was taken as tubulin is a labile protein and thus requires to immediately be frozen in liquid nitrogen and stored at $-80°C$ and used immediately after thawing to maintain its activity.

- Various polymerization enhancing components were tested such as glycerol, methyl cellulose, and DMSO.

- Application of nucleation seeds, typically $\ll 1\mu m$ preformed microtubules stabilized by taxol or GMPCPP to circumvent possible undisclosed errors at the nucleation step. Such seed in essence only should speed the polymerization process up without changing it, see protocol below.

- A number of different protocols suggesting centrifugation, stepwise dilution, polymerization in chamber or in tubes etc.

- A thorough investigation of the parameter-space of concentrations, incubation-time and -temperature.
- All components were replaced and a couple of different buffers tested.
- A visit at the AMOLF institute in the Netherlands at the laboratory of the research group of Marileen Dogterom who specialize in microtubules, was done to resolve the issue of failed tubulin polymerization. The visit did produce the desired microtubules and can be seen in figure 4.1. It is based on the following protocol, where at first tubulin is polymerized in the presence of GMPCPP forming small $\approx 1\mu m$ stable microtubules of which a small amount is then added to a general GTP containing polymerization mix.

  - **Seed solution**, store a room temperature.
  - $2.4\mu L$ Tubulin @ $100\mu M$ + $0.6\mu L$ Biotin-Tubulin @ $10\mu M$
  - $1\mu L$ GMPCPP @ $10\mu M$ + $1\mu L$ BRB80
  - Incubate at $37°C$ for 20-40 min, then dilute with e.g $45\mu L$ BRB80

  - **Polymerization mix**
  - $3.0\mu L$ Tubulin @ $100\mu M$ + $4.5\mu L$ GTP @ $1mM$
  - $5.5\mu L$ BRB80
  - $1\mu L$ Methyl cellulose (1%) + some seed solution
  - Incubated directly at sample at room temperature

  It was however not possible to reproduce the results using the same protocol at NBI.

Taxol polymerization

Taxol stabilized microtubules are in the literature simply polymerized as above but in the presence of taxol, or suspended in a solution of taxol after an initial polymerization period. Instead of the expected solution of individual microtubules, the microtubules of this project self-organized in large asters or bundle like formations. These are shown in figure 4.2

These formations were typically similar within each prepared polymerization solution and present in abundant numbers. However, single ones as the one shown in figure 4.2:G, would only be found very infrequently. What unfortunately was not evident from the beginning was that these formations

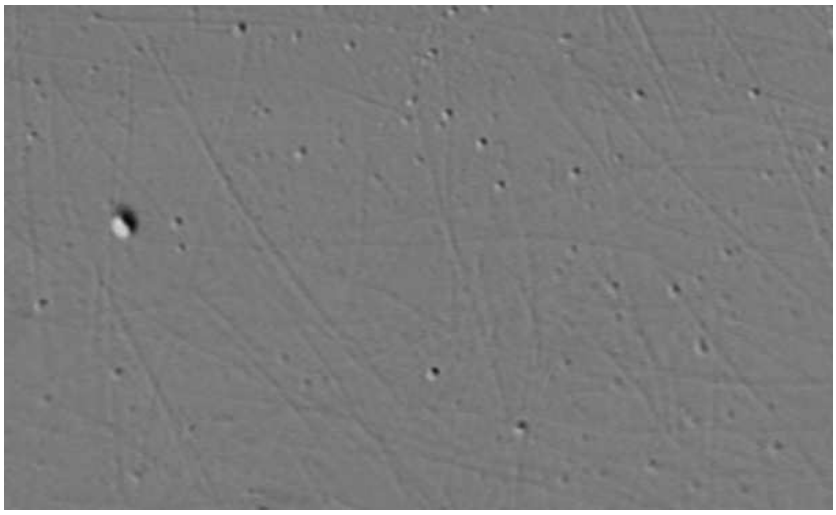

Figure 4.1: ×63 DIC Pictures of dynamic selfassembled microtubules at the coverslip.

are not MTOC's or some other special microtubule structures, but taxol crystals or taxol crystal partly covered with tubulin. In virtually all *in vitro* experiments using taxol as a stabilizing agent, it is used in a concentration of $20\mu M$. Taxol, dissolved in DMSO, has a solubility of in aqueous solution of $0.77\mu M$ and hence precipitation is expected and some literature does suggest a number of protocols or tricks to handle this. One observation is that at high enough concentrations the asters would seem be more dense if left to polymerize for a longer time as a difference as seen comparing figure 4.2: A and B. Another observation was probably a more traditional precipitation of taxol, as the solution observed through the microscope would seem to have a higher viscosity or grainy texture. On a couple of occasions a few taxol formations were found under the latter conditions as well, but never in abundant numbers. The final step in concluding that it indeed was taxol crystals was when the formations were found in solution containing no tubulin, see figure 4.2:E.

The formation of taxol asters and bundles at typical concentration of both *in vivo* and *in vitro* experiments was documented in [14] and subsequent how they can be coated with tubulin or other proteins, suggest an alternative binding site in [9]. The authors of these findings encourage the readers to review and rethink previously experiments involving taxol both *in vivo* and *in vitro*. These studies were published during the timespan of the experiments of the current project.

An interesting observation of the found taxol crystal was done in a transmission electron microscope, see figure 4.3. Clearly the taxol crystal has a

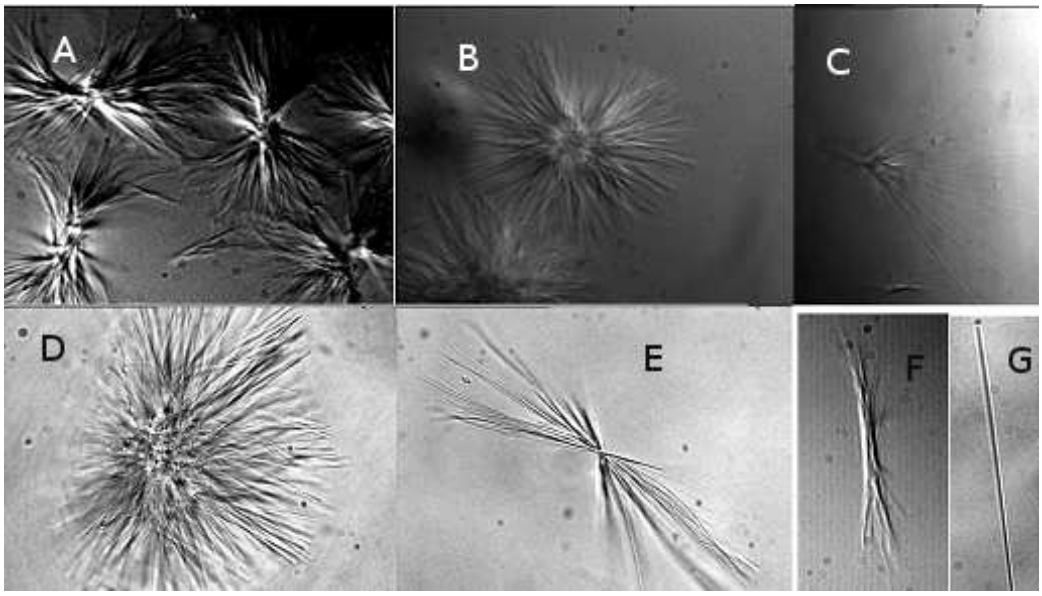

Figure 4.2: DIC pictures of the various asters,bundles and occasional singles observed in solutions containing Taxol at NBI.

needlelike appearance and might be conceived as bundles of such needles. This is especially interesting in respect to the behavior found by Pamploni et al. of taxol stabilized microtubules, when reviewing this through bundle mechanics. The final attempts to produce microtubules suitable for persistence length determination, as the above described, was done with preformed taxol stabilized microtubules from Cytoskeleton inc. of average length $2\mu m$. As this procedure also failed and eventually pure taxol crystals were found, the work was abandoned.
99% pure bovine tubulin was purchased at Cytoskeleton inc., GMPCPP from Jena Bioscience, other components DTT, glycerol, methyl cellulose, DMSO etc. all from Sigma Aldrich. Taxol was purchased both from Sigma and Jena. Tubulin as the central components was reordered several times, these restocks were on occasions from the same original stock of the supplier.

4.2 TPPP/p25

The only truly successful polymerization of microtubule in this project was in the presence of the protein TPPP/p25 or unabbreviated Tubulin polymerization promoting protein $p25\alpha$.

The $25kDa$ heavy TPPP/p25 was the first discovered in a recently established family of proteins found in vertebrates, other members include

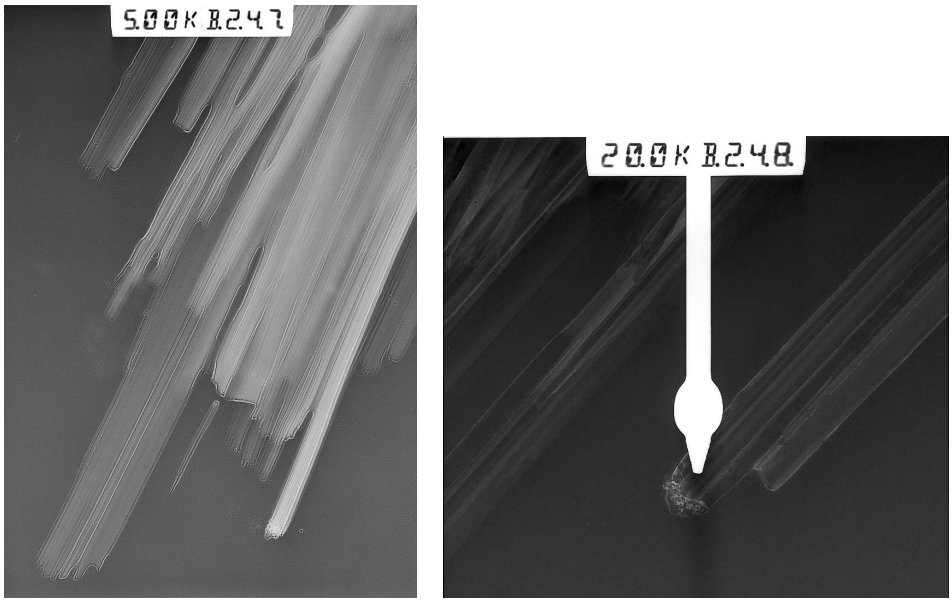

(a) $\times 50k$ (b) $\times 20k$

Figure 4.3: TEM pictures of pure taxol crystals at 50k left and right 20k magnification. The white region in (b) is a pointer of the TEM for measuring distance and as such an artifact in this particular picture.

TPPP2 and TPPP3, but only TPPP/p25 is common throughout the animal kingdom. It binds/ascociates both to free tubulin as well as to fully formed microtubules. It can therefore be classified among the microtubules associated proteins MAP's. As the name suggest TPPP/p25 promotes the polymerization of tubulin, effectively lowering the required critical concentration. Through a stabilizing effect on microtubules it also hinders catastrophes. This promotion of polymerization might be oligomeric in nature, as $3-4$ tubulin subunits bind per TPPP before these oligomers assemble into larger microtubules and microtubules superstructures. The association of TPPP/p25 to tubulin or microtubules is competitive with the association of GTP, thereby suggesting a shared binding site. TPPP/p25 induces polymorphic microtubules structures at an extended rate, primarily seen as a rise in the formation of double walled microtubules and microtubule bundles [43] [18].

TPPP/p25 is, like other MAP's, an unstructured protein. Unstructured means that it possesses no specific secondary or tertiary structure, although parts of it might be natively folded [25]. The unfolded and disordered part is an N-terminal tail and distinguishes it from the lighter members of the TPPP family such as the human homologs TPPP/p18 and TPPP3/p20; both found

to influence tubulin polymerization to lesser and different extent, and hence the N-terminal tail is believed to be the key factor for interaction.

It is a brain specific protein expressed mainly in the oligodendrocytes, but TPPP orthologs are also among the only 16 genes that can be found in all ciliated organisms, suggesting that TPPP may be associated with a basic function of cilia [36]. It is therefore very likely to be strongly related and involved with the centrioles and centrosome matrix.

The principle function of oligodendrocytes is to provide structural support to the axons in the central nerve system and produce the insulating myelin sheaths surrounding them. Oligodendrocytes form segments of myelin sheaths at numerous neurons at the same time as it wraps itself around them, leaving a fresh formed myelin sheath behind. The oligodendrocytes will in addition to the wrapping also migrate along the axons and thereby completely inclose them in a myelin sheath.

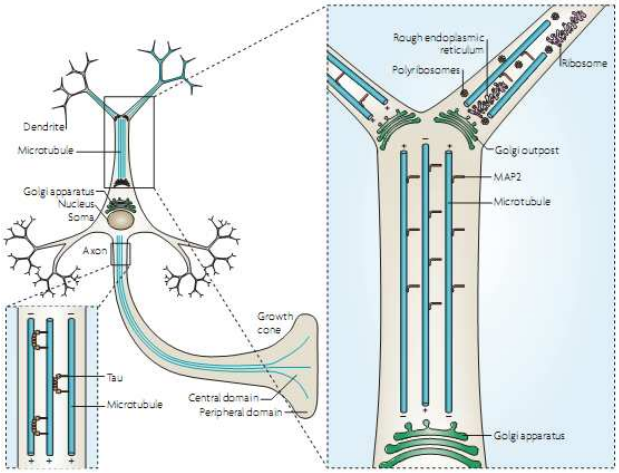

Figure 4.4: Microtobules in axons and dendrites, where MAPs including tau bundle them in different formations.

Pathological conditions

The stabilizing effect of TPPP/p25 on microtubules and the following effect on mitosis may be crucial for the proliferation of neoplasmic cells. The expression of TPPP/p25 in fully matured oligodendrocytes is much higher than in their precursors, the oligodendrocyte progenitors cells. But is not found in neoplastic oligodendrocytes, i.e. cancer cells. This leads to the believe that such neoplasmic cells are developed as either the progenitor cells never develop the ability to properly express TPPP/p25, or that the genes of

TPPP/p25 in mature oligodendrocytes are suppressed or altogether silenced. A mutation in cancerous oligodendrocytes leading to a rapid degradation of TPPP/p25 could also be an explanation. but the mechanism and causality of lack of TPPP/p25 necessary leading to the formation of neoplasmic cells is yet to be established.

The lack of TPPP/p25 is, as stated above, related to the proliferation of neoplasmic cells. Interestingly, over-expression might also lead to pathological conditions. As seen in Figure 4.5 the over-expression of TPPP/p25 will lead to the formation of a closed microtubule network within the cell. The pictures clearly show how the microtubules in the HeLa cells expressing eGFP-TPPP/p25 (yellow) form an aggresome and/or a perinuclear cage. Aggresomes are protein inclusions bodies at or around the centrosome, and are typically observed in stressed cells experiencing failure somewhere in the protein degradation pathway. Inclusion bodies as these are found under various pathological conditions and specific for TPPP/p25. Including myelin sheet disruption and accumulation of TPPP/p25 within cytoplasmic inclusions detected in Multiple System Atrophy, MSA [53], as well as in the Lewy bodies of Parkinsons and 'diffuse Lewy body disease'. In the later case TPPP/p25 is believed to provide the link between the non tubulin interacting α-synclein, which is the key molecule of Parkinson and microtubules. The over-expression of TPPP/p25 with accompanied cage formations and shutdown of microtubules dynamic will eventually lead to cell death [31].

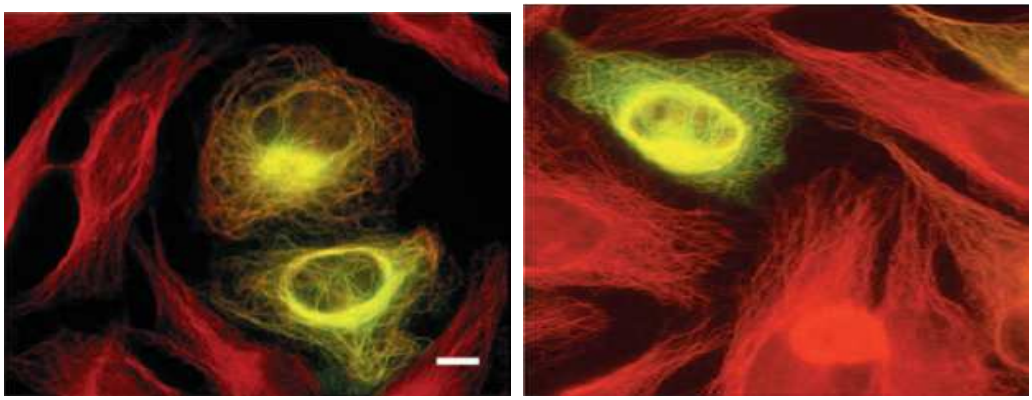

Figure 4.5: HeLa cells: Yellow (false colour) is expression of bovine eGFP-TPPP/p25. Cells expressing TPPP/p25 where found to form perinuclear cages or other sort of aggresomes of microtubules. Pictures from [31].

4.3 *In vitro* microtubules networks

The TPPP/p25 used in the experiments of this project is the bovine homolog which is 90% identical to the human. It was provided through the research group of Judit Ovadi PhD. D.Sc. institute of Enzymology of the Hungarian Academy of Sciences in Budapest. It was, and should be, handled in a similar manner as the tubulin.

In the experiments presented here it was observed that even under *in vitro* conditions tubulin polymerized in the presence of TPPP/p25 would form large networks, and not solutions of individual microtubules, see figures 4.6 and 4.7. As the network images reveal the microtubules are often curved which is not normally the case for *in vitro* polymerized microtubules, but corresponds well with the *in vivo* cage formations. Notice the large centrosome-like hub from where the microtubules seems to originate from. There is some resemblance of these centrosome-like hubs and the taxol asters of figure 4.2. This did also not simplify the process of abandoning the taxol polymerization process. Further investigation was done on these networks.

The recipe for microtubule polymerization by TPPP/p25 was as simple as possible:

- $2.0\mu L$ Tubulin @ $100\mu M$
- $18\mu L$ BRB80
- $1\mu L$ TPPP/P25 @ $10mg/mL$

Simply mix and let polymerize directly in the sample chamber at $\approx 37^oC$. The process of producing these networks was in periods halted due to the supplied TPPP/p25 being in a nonactive form and the supply scarcely. It might not have been appropriately folded or incomplete lacking residues.

It is evident from figure 4.8 that there is no resemblance of the taxol crystals and TPPP/p25 polymerized microtubules when viewed by transmission electron microscopy, TEM. A staining procedure necessary to observe microtubules by TEM can be found in the appendix.

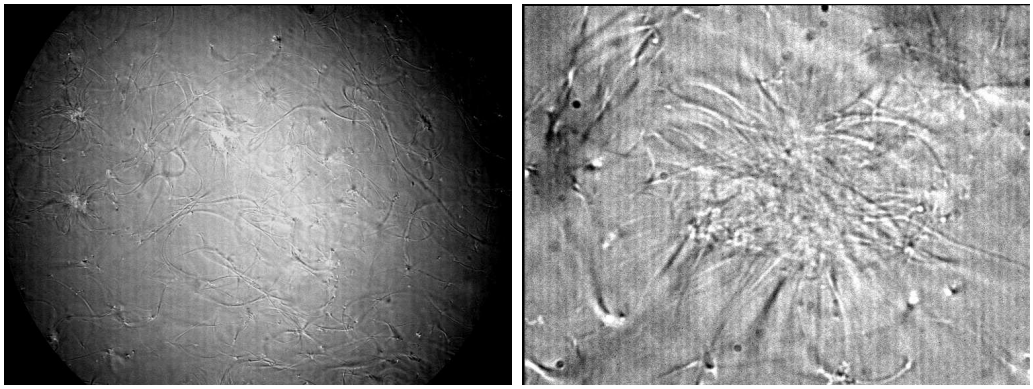

Figure 4.6: DIC pictures of microtubule network formed with TPPP/p25. *left:* overview at ×63. *right:* Close up of one of the centrosome-like hub structure typical of the polymerized networks.

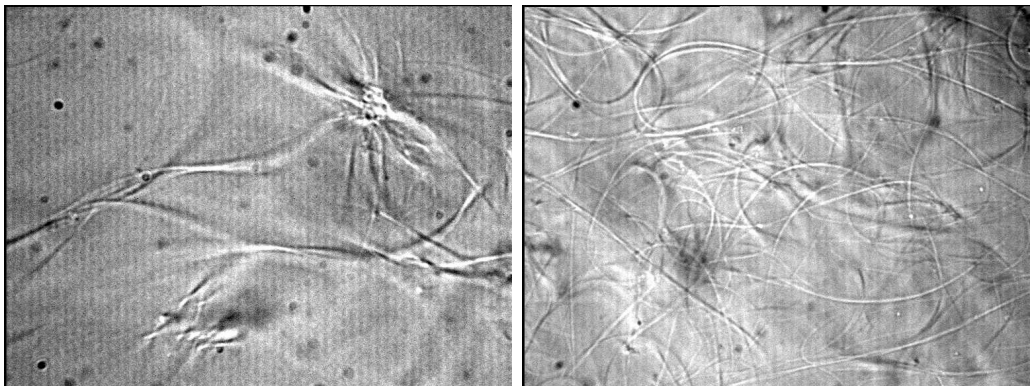

Figure 4.7: DIC pictures of microtubule network formed with TPPP/p25. *left:* Another but not so dense hub structure. *right:* The curved quality is evident

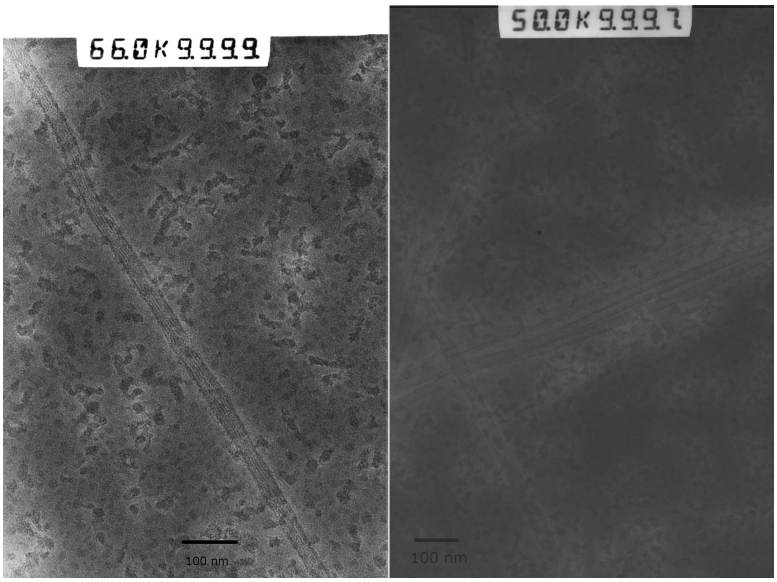

Figure 4.8: TEM pictures of microtubules polymerized with TPPP/p25. *left:* One single microtubule from top left corner to lower right, 66k magnification. It is possible to resolve aa striped appearance (protofilaments). *right:* Several crossing each other at 50k magnification.

Chapter 5

Polymer networks

Solutions of polymers or polymer networks are complex fluids. The properties of such solutions still reflect the basic mechanical properties of the polymer, but in addition also receive properties due to their interactions. This means that quantities such as concentration and tendency to crosslink will become important. Complex fluids can in general by said to be viscoelastic, as they both dissipates(viscous) and and stores energy(elastic). The more the polymers crosslink the more elastic the response of the network will in general be. Polymers that does not crosslink still interact by friction. Thus the response is always based upon the concentration of polymers- the number of interactions must grow with increasing concentration. Clearly the overall number of interactions, be it friction or crosslinking, is also governed by the length to persistence length ratio of the polymers. $l \gg L_p$ must give more interactions than if $l \ll L_p$.

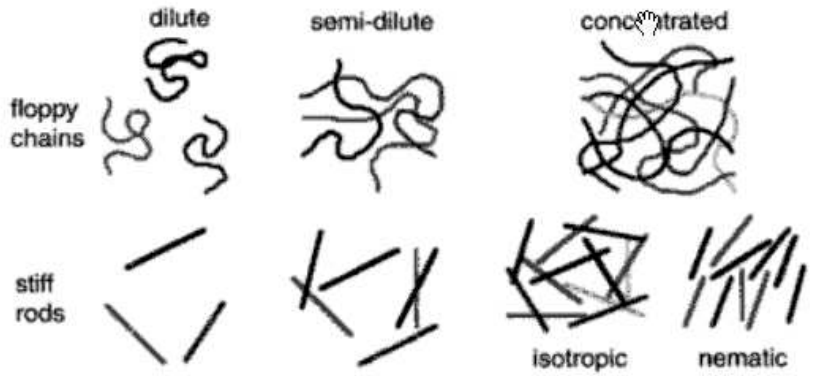

Figure 5.1: Appearances of polymer solutions, with varying degree of interaction. Typically the semi-dilute regime is the biological relevant. Figure from [4].

5.1 Microrheology

The study of the response of materials to strain or stress is known as rheology. Of special interest is a relatively new method called microrheology, where such solution as polymer networks, are characterized by observation of small tracer particles and quantified by the mean squared displacement of these:

$$\langle \Delta \mathbf{r}(\tau)^2 \rangle = \langle (\mathbf{r}(t+\tau) - \mathbf{r}(t))^2 \rangle, \tag{5.1}$$

where $\mathbf{r}(t)$ is the position at time t, and τ the lag time. Tracer particles are as a rule beads (spheres). The relation of the mean squared displacement and the response of the material can be visualized by the two extreme cases of a purely viscous fluid and a completely elastic material:

A: viscous fluid

Diffusion is probably best know through the diffusion equation used from economics to physics and chemistry:

$$\frac{\partial}{\partial t} c(\mathbf{r}, t) = D \nabla^2 c(\mathbf{r}, t), \tag{5.2}$$

$c(\mathbf{r}, t)$ a probability for finding a given quantity at time t and place $\mathbf{r}$ and D a diffusion constant. The diffusion equation operates with probability distributions and describes the behavior of ensembles of particles rather than the motion of the individual particle. The underlying dynamic is that the individual behavior of particles is uncorrelated, random. For diffusion concerning particles and concentrations, as here, random must mean that inertial forces are dominated by viscous forces as they otherwise would direction biased. The ratio of viscous and inertial forces is given by the dimensionless Reynolds number:

$$Re = \frac{\mathbf{F}_{inertial}}{\mathbf{F}_{viscous}} \approx \frac{\rho v L}{\eta}. \tag{5.3}$$

ρ density, v it's characteristic speed through the media, L characteristic size of particle and η the viscosity. The Reynolds number thus must be small to fulfill the requirement for the motion to be random. This lead to the following equation of motion:

$$\mathbf{F} = \sigma \dot{\mathbf{r}}, \tag{5.4}$$

σ the mobility. The force acting on a particle will originate from the momentum transfer from the many collisions with solvent particles having energy

according to equipartition. Now, if we observe such a particle undergoing many collisions, we will find that it follows, a very irregular but continuous path. This motion is called Brownian motion, and when taken into account the very high frequency of particle collisions and very small intercollision travel lengths, we can describe is as the limit of a random walk with infinitesimal and independent steps.

If we look at a random walk in one dimension (x) without any external forces, we have a probability that is unbiased and independent of other particles $p = \frac{1}{2}$ for each particle to go in either direction $\pm x$. They will do so on average for every amount of time t that passes, and travel a distance l in the $\pm x$ direction, this is considered a step. Lets look at N particles, we will assume they all start out at time ($t = 0$) and at position $x = 0$. After n steps the ith particle has a position $x_i(n) = x_i(n-1) \pm l$, the mean position of the N particles is then given by:

$$\langle x(n)\rangle = \frac{1}{N}\sum_{i=1}^{N} x_i(n) \Rightarrow \langle x(n)\rangle = \frac{1}{N}\sum_{i=1}^{N}(x_i(n-1) \pm l) \tag{5.5}$$

the term $\pm l$ returns zero when summing due to the equal probability of the two directions, which yields:

$$\Leftrightarrow \frac{1}{N}\sum_{i=1}^{N}(x_i(n-1) = \langle x(n-1)\rangle \Rightarrow \langle x(n)\rangle = \langle x(n-1)\rangle, \tag{5.6}$$

i.e the mean position of the particles does not change, but the particles spread. The measure of the spread $\langle x^2(n)\rangle$ is easily found going through the same calculations

$$x_i^2(n) = (x_i(n-1) \pm l)^2 = x_i^2(n-1) \pm 2lx_i(n-1) + l^2$$

$$\Rightarrow \langle x^2(n)\rangle = \frac{1}{N}\sum_{i=1}^{N} x_i^2(n-1) \pm 2lx_i(n-1) + l^2 = \langle x^2(n-1)\rangle + l^2 \tag{5.7}$$

resulting in: $\langle x^2(n)\rangle = nl^2$ Finally expressing n as a function of time $n = \frac{t}{\tau_0}$ and introducing a constant $D = \frac{l^2}{2\tau_0}$ we obtain: $\langle x^2(t)\rangle = 2Dt$. The constant D is the diffusionconstant. Expanded into 3 dimensions we have :

$$\langle \mathbf{r}^2(t)\rangle = 6Dt \tag{5.8}$$

given that the probability also here is independent of other particles and unbiased in each direction [2].

So we find for a viscous fluid, that the mean squared displacement is proportional to the diffusion constant. Since we have assumed to be under conditions of a low Reynolds number we can use Stoke to find the viscosity:

$$\eta = \frac{k_B T}{6\pi D a} \tag{5.9}$$

with a being the radius of the particle. Hence we have a connection of the mean squared displacement and the properties of a viscous fluid.

The diffusion equation and corresponding description of brownian motion dates back to Einstein in the beginning of the 20th century (1905).

B: elastic material In the other case of an elastic material the bead is constrained and the mean squared displacement must reach some maximum $\langle \Delta r^2_{max} \rangle$. By representing the elastic response of the surroundings with an effective spring constant and equating it with the thermal energy of the of the bead:

$$\frac{1}{2} k \langle \Delta r^2_{max} \rangle \sim \frac{1}{2} k_B T, \tag{5.10}$$

we obtain a relation between a material constant and the mean squared displacement. Figure 5.2 display the two cases of purely a viscous and purely elastic response.

Microrheology is either done passively or by driving the bead through the solution. To emphasize, the response of a viscoelastic material is in its nature dependent on the timescales upon which it is observed. Introduced stress will diminish with time. The method used to observe this phenomena must naturally reflect this, and the mean squared displacement will in the general case have an nontrivial dependence on time, as is also the case for the constrained movement in figure 5.2. In general the "spring constant" is related to the elastic modulus G of the viscoelastic fluid through a characteristic length (bead radius), and the full frequency dependency of this modulus can be obtained through the la place transform of the mean squared displacement $\langle \tilde{r}(s) \rangle$, by use of a generalized Stoke-Einstein equation [34]:

$$\tilde{G}(s) = \frac{k_B T}{\pi r s \langle \tilde{r}(s) \rangle}, \tag{5.11}$$

s the La place frequency. However, this is not directly the method used in the experiments of present text. It will also be problematic to use this Stoke-Einstein relation for timescales where the MSD(τ) tends to be curved.

Another variation is 2-point microrheology where the correlation of the movement of two tracer particles is observed. It may seem appropriately here to remind that a mean squared displacement can be the mean of both a an ensemble as well as the time average of one particle introduced above. The typical method of observation in microrhelogical experiments is through analysis of images obtained by high speed cameras capable of upwards 1000 frames per second.

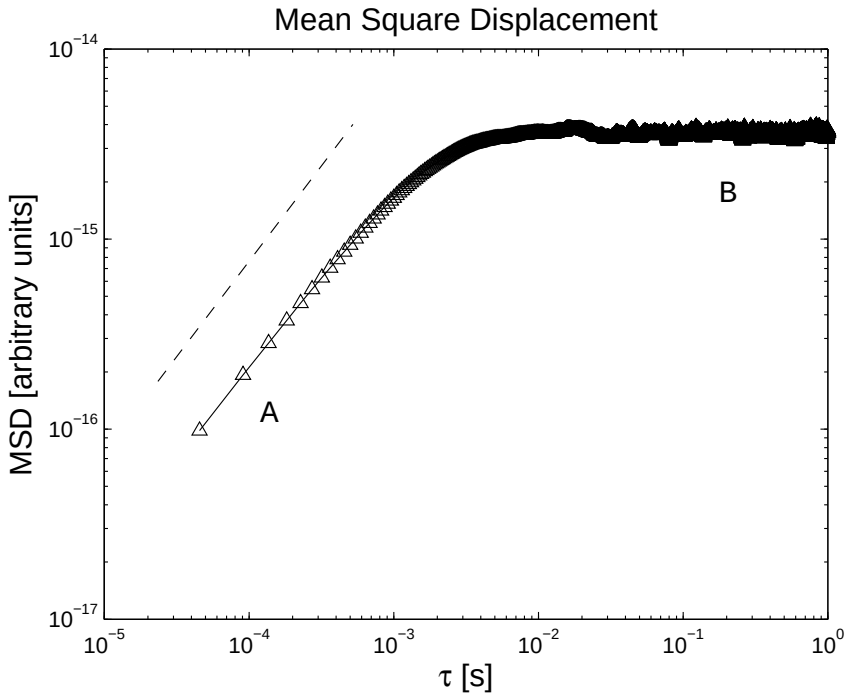

Figure 5.2: Matlab simulation of particle trapped in harmonic potential based upon a correlation as described in (19) [3]. The slope of the dashed line is 1. *A* Purely viscous response or free diffusion. *B* The response is purely elastic.

5.2 Coefficient of diffusion

If we look at the mean squared displacement considering these two cases where the mean squared displacement of a tracer bead will either be proportional to τ in the viscous case, or constant in the elastic case. Formally it can be stated, that given a viscoelastic fluid, the logarithmic time derivative of the mean squared displacement

$$\langle \Delta \mathbf{r}(\tau)^2 \rangle \propto \tau^{\alpha}, \tag{5.12}$$

will have a value between one and zero.

We can characterize the diffusion by this power exponent α. A coefficient $\alpha = 1$ characterizes normal diffusion and a value $\alpha < 1$ is termed subdiffusion, as the movement is soehow restrained. In the case $\alpha > 1$ we observe superdiffusion, where the movement is enhanced. An example of superdiffusion is the transport of vesicles by kinesin along microtubules but can also be observed when a flow or a gradient is present. Examples of subdiffusive processes could be a particle diffusion on a cellmembrane, that is a on a 2D plane in 3-dimensional space or diffusion in gels or polymer solutions and viscoelastic materials in general. Theoretically all kinds of diffusive processes when reviewed at timescales short enough should have the diffusion to appear ballistic $\alpha = 2$, dominated entirely by inertia.

For polymer solutions the typical experimental determined coefficient is $\alpha \approx 0.75$, among several: *in vitro* (microtubules) [7] and *in vivo* (complete yeast cell networks) [44]. It is theoretically derived by assuming that movement of the bead embedded in the polymer network is precisely equal to the movement of the polymers and solving the hydrodynamic equation 3.18 of chapter 3. This is done in e.g [7] by Caspi et al. using fixed boundary conditions:

$$\langle \Delta y^2(x,\tau) \rangle = \frac{4}{l} \sum_{n=1}^{l/a} \frac{k_B T}{EIq^4} (1 - e^{w(q)}) sin^2(qx), \tag{5.13}$$

q the wavenumber $q = \frac{n\pi}{l}$ and w the relaxation rate (reverse relaxation time).

For short timescales the solution reduces to:

$$\langle \Delta y^2(x,\tau) \rangle = 0,041 \left[ln \left(\frac{EI \cdot \tau \cdot ln(l/\pi a)}{4\pi\eta a^4} \right) \right]^{3/4} \times \left(\frac{k_B T}{\eta} \right)^{3/4} \frac{1}{L_p^{1/4}} \tau^{3/4} \tag{5.14}$$

$$\propto \frac{K_B T}{\eta^{3/4} (EI)^{1/4}} \tau^{3/4} \tag{5.15}$$

Notice the dependency of the persistence length and the practically independence of the length l. For long timescales:

$$\langle \Delta y^2(x,\tau) \rangle = \frac{2}{3} (\frac{x}{l})^2 (1 - \frac{x}{l})^2 \frac{l^3}{L_p}, \tag{5.16}$$

we have the completely elastic response and the value is strongly depended on the length of the polymer.

For the above to be true, it is essential that the bead is in constant and total contact with the polymer, and the mesh size of the network therefore

must be small enough, such that the bead cannot jump/ diffuse freely around. The TPPP/P25 microtubule networks produced in the experiments of this text would have unknown mesh size. This possible source of error was circumvented by binding the beads to the microtubules. Attaching the bead makes it possibility and a priority to observe for anisotropy of the movement in respect to a transverse and a longitudinal direction. If the measured bead only reflects the behavior of one bundle of or a single microtubule, the movement would be as found above for the transverse direction, whereas for longitudinal direction, it with the approach used above, must be expected to behave as freely diffusing, as long as there are no further interactions. If the measured bead on the other hand reflects the behavior of a network the movement would be identical and described by equations above for all directions. Intrinsically in above consideration lies the persistence length of microtubules. To define a transverse and longitudinal direction the polymer must seem as rigid on the scale of the observed movement. For a polymer that would appear floppy on the same scale, such polymer related directions can not be defined, and neither would a difference in movement be expected in respect to any coordinatesystem.

Power spectrum

If we look at equation of motion for the a freely diffusive particle where we established that MSD scaled with $\alpha = 1$

$$m\ddot{x}(t) = -\gamma\dot{x}(t) + F(t), \tag{5.17}$$

$F(t)$ representing the force of collision and γ is the drag coefficient. Let $\tilde{x}$ be the fourier transform of x and ω the frequency. We can write the power spectrum:

$$\langle\tilde{x}(\omega)^2\rangle = \frac{\langle\tilde{F}(\omega)^2\rangle}{(2\pi\gamma)^2\omega^2} \Rightarrow \langle\tilde{x}(\omega)^2\rangle \propto \frac{1}{\omega^2}, \tag{5.18}$$

where we incorporate that the force from collision must be random such that $\langle\tilde{F}(\omega)^2\rangle$ is constant ($= 4\gamma k_B T$). (white noise)

If we add an additional force into the equation of motion and thereby restrict the movement, we will be in the subdiffusive regime, the power exponent of the frequency will reflect this, and it can be shown, for a limited frequency range [40]:

$$\langle\tilde{x}(\omega)^2\rangle \propto \frac{1}{\omega^{1+\alpha}}. \tag{5.19}$$

Provided a timeseries of the position we thus have and additional method to extract the exponent $\alpha$and thereby characterize the diffusion. In the case

where the additional force is from a harmonic potential, such as an optical trap of spring constant k $\omega_0^2 = \frac{k}{m}$ the power spectrum is given as:

$$\langle \tilde{x}(\omega)^2 \rangle = \frac{\langle \tilde{F}(\omega)^2 \rangle}{(2\pi\gamma)^2(\omega_c^2 - \omega^2)} = \frac{D}{\pi^2(\omega_c^2 - \omega^2)}, \tag{5.20}$$

where ω_c is the corner frequency $\omega_c = \frac{k}{2\pi\gamma}$ [3], and in the last step we used the definition 5.9. This corner frequency is a charecteristic for distinguishing between the bead being in a restrained or free regime. For frequencies $\omega \gg \omega_c$ (small time steps) the particle behaves as freely diffusing, while it in the other case $\omega \ll \omega_c$ the particle is restrained. This is the basis of calibration of the optical trap where the position is reported as a potential. Timeseries of the photodiode potential are fourier transformed and the corner frequency, and thereby the the spring constant is found by fitting of above equation, which incorporates the viscosity and temperature of the fluid. Equating the thermal energy with the spring energy as in equation 5.10 an expression for the mean square $\langle x^2 \rangle$ is obtained. By comparing this to the variance of the position distribution, which for a gaussian (centered around zero) distribution precisely is the mean squared position, a conversion factor between the two values therefore exists. This of course prerequisite that the potential of htm photodiode is linear with the actual movement of the trapped object. Calibration is, however, not essential for the experiments of the present text, as it is the power exponent α that is the focus of interest. This omission of calibration is the reason that reported values of MSD(τ) appears as square volts rather than square meters. Data was, however, compared to equation 5.20 to insure that beads perceived as free indeed also were free. For calibration and observation of freely diffusing beads see [3].

The analytical solution

The previous mentioned Stokes-Einstein relation of viscoelastic properties and the la place transform of the mean squared displacement in equation 5.11, is derived based upon a langevin without a term to specifically account for the optical trapping. In a recent paper 2009 [11] by Desposito and Vinales, an exact analytical solution of the mean squared displacement for a bead embedded in a viscoelastic material, such as a polymer solution, and also subjected to a harmonic potential of a optical trap, was derived. Without going into details, it is here presented:

$$\langle \Delta r(\tau)^2 \rangle = \rho(\tau) = \frac{2k_bT}{m} \sum_{k=0}^{\infty} \frac{(-1)^k}{k!} (\omega_0\tau)^{2k} \tau^2 H^k_{2-\lambda,1+\lambda k}(-\gamma_\lambda \tau^2 - \lambda), \tag{5.21}$$

$H_{\alpha,\beta}(y)$ are generalized Mittag-leffler functions, $0 < \lambda < 1$ a subdiffusive coefficient and γ in this context best thought of as damping or "memory". For short timescales behavior they find:

$$\langle \Delta r(\tau)^2 \rangle = \frac{k_B T}{m} \left(\tau^2 - \frac{2\gamma_\lambda}{\Gamma(5-\lambda)} \tau^{(4-\lambda)} - \frac{\omega_0^2}{12} \tau^4 \right), \tag{5.22}$$

where Γ is the gamma function. We can see the ballistic behavoir τ^2 for smallest timescale. Please view figure 5.3.

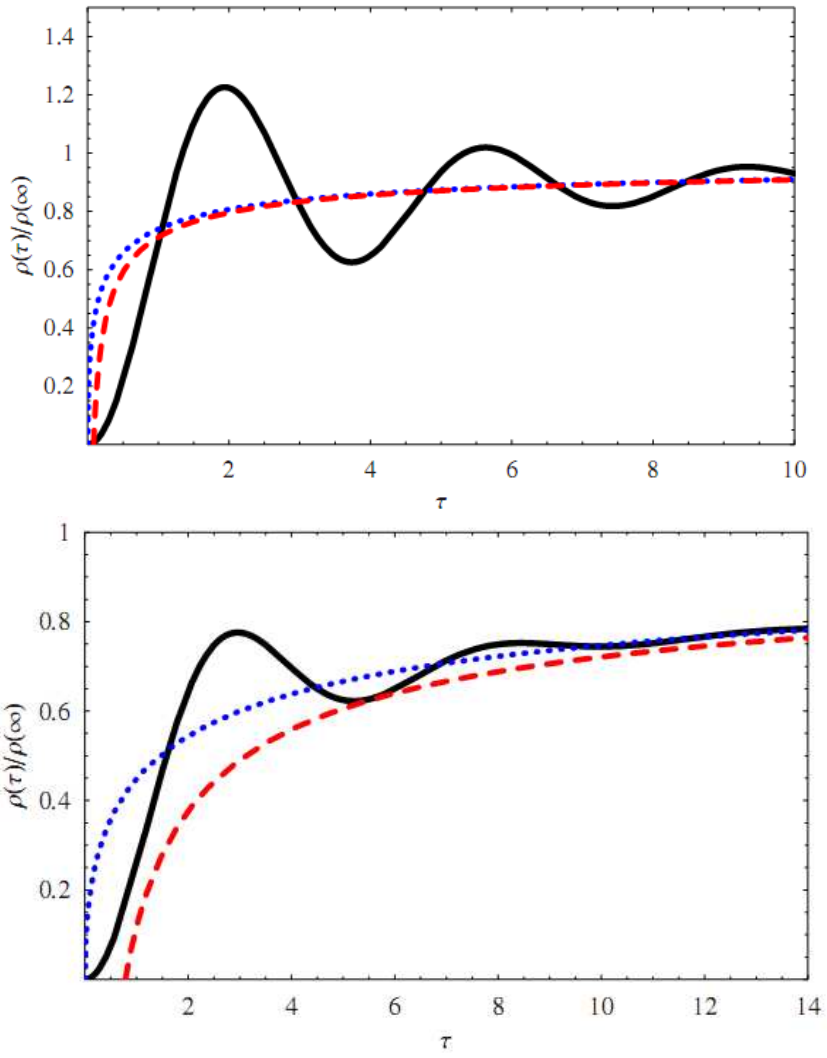

Figure 5.3: Normalized mean square displacement, here ρ. Black line represent the exact solution, blue and red dashed are approximations. The conditions are identical except for the used trap frequency: *top:* $\omega_0 = 1.4$, *bottom:* $\omega_0 = 0.8$ [11].

At small timelags we observe a step rise to the asymptotic value used for normalization. The solution is clearly oscillatory with an decreasing amplitude for growing timelag τ. The analytical solution agrees with simulations, but is not compared to experimental data by Desposito and Vinales.

Chapter 6

Methods

In previous chapters the optical trap has been appearing as mean for manipulation and/or a tool for measuring force and displacement without proper introduction. An optical trap or a pair of optical tweezers is the creation of a $3D$ harmonic potential confining some trapped object. This chapter tries to briefly outline how optical trapping can be explained, and introduces the experimental setup used to manipulate and measure including used microscopy methods.

6.1 Optical trapping

So how does light catch anything apart from paralyzing animals in the headlights of cars?

Light is quantifiable not only in terms of energy, but also perhaps somewhat more intriguingly in terms of momentum. This momentum can, as always, be transferred or gained under interaction with the surroundings and light thus can exert force. Now we do not normally experience the momentum of light for instance do we not feel a sudden radiation pressure from turning on a lightbulb when entering a room, but we do indeed feel the energy absorbed in the skin on a sunny day. The relation between energy E and momentum p for the massless light is familiar from relativity:

$$E^2 = p^2c^2 + m_0^2c^4 \Rightarrow E = pc. \tag{6.1}$$

The moment is most often expressed as:

$$\Rightarrow p = \frac{E}{c} = \frac{hv}{c} = \frac{h}{\lambda}, \tag{6.2}$$

where h is plancks constant, c the speed of light in vacuum, and λ the wavelength.

As stated above the forces exerted by light is small and generally lies in the femto- to piconewton range. These forces are, however, considerable for microscopic objects and sufficient to keep them trapped. The full explanation of optical trapping is beyond the scope of this project and to some extent rather complex. Instead the two limiting cases for objects of diameter d much larger, $d \gg \lambda$, than the wavelength and for when the diameter is considerable smaller than wavelength will be outlined. In the first case, what is sometimes termed the ray optics regime, conventional ray considerations can provide a somewhat satisfactory and intuitive explanation and, in the later, Rayleigh regime, the well known electromagnetic description of light provide an equally reasonable explanation. For microscopic objects to be trapped they have to fulfill following conditions: They must be electrically polarizable, they have to permit transmission of light through them and have a refractive index higher than the surrounding media. In addition thereto the trapping laser most have some sort of non constant intensity profile to provide a gradient in the electric field. This is not the equivalent of an unstable laser. In the following the laser is assumed to be in TEM_{00} mode and thereby have a 2D gaussian energy intensity profile with maximum in it's center and the trapped microscopic object to be a sphere or bead.

Ray optics regime ($d \gg \lambda$)

Here a traditional Ray optic approach is applicable. Incoming light will be refracted twice once at the interface media-bead entering the bead and once at the bead-media interface as it exits the bead. Refraction from higher to lower refractive index, as in the case at hand, is towards the surface normal and vice versa. Both transmissions are in accordance with Snell's deflection law:

$$n_s sin(\theta_s) = n_o sin(\theta_o). \tag{6.3}$$

The indices "s" and "o" refers to the surroundings and trapped object respectively, and n is the refractive index and the angle θ is in respect to the normal of the interface between surroundings and the object. The incoming light rays will thus exit in a different direction and it's momentum is thereby changed. This change must be counter acted by an equal but opposite change of the momentum of the bead according to Newton's 3. law. Due to the laser intensity profile providing more rays and hence a larger transfer of momentum at the center of the beam, any lateral deflection from the beam center of the bead will be counteracted by an increase of restoring momentum. The momentum induced on the bead from the light will also point towards a cen-

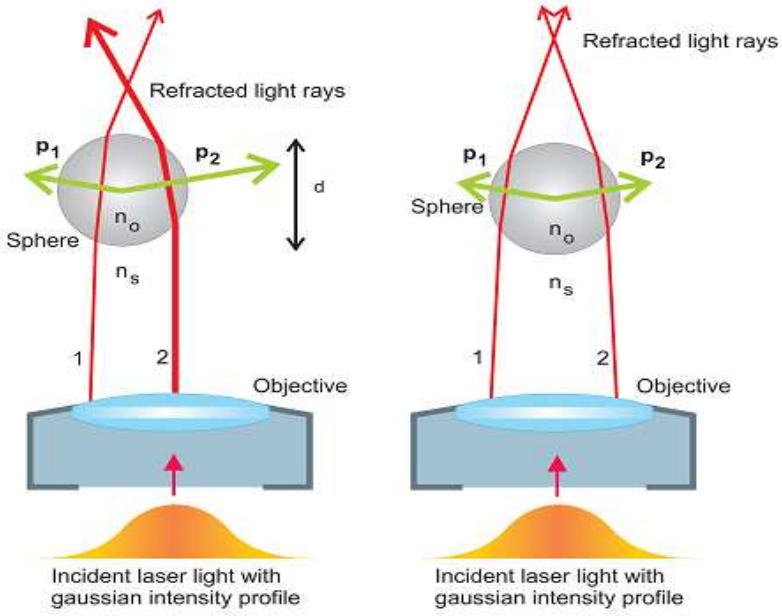

Figure 6.1: Ray optic approach to understanding optical trapping for ($d >> \lambda$). $n_0 > n_s$ and the presented momentum p_1 and p_2 are those belonging to the bead. *Left:* Lateral trapping, any deflection from the intensity center gives rise to a restoring momentum *Right:* Trapping in the axial direction. If one imagines the rays propagation in the opposite direction, corresponding to a bead placed behind the focal point, it should be clear that the bead indeed is also trapped. Figure curtesy of Dejan Trpcevski [46].

ter in the axial direction, a.k.a. the focal point, if the laser beam is focussed by a lense. Figure 6.1 displays the resulting momentum of the bead.

Rayleigh regime ($d \ll \lambda$)

In this limit we can treat the polarized bead as a point dipole and the laser by it's electromagnetic description as an electric field. The transverse intensity of the laser is as already mentioned Gaussian and is furthermore also focused by a lens, this evidently leads to an electric-potential-field gradient both in the lateral and in the axial direction. This means that the bead must be subject to Lorentzforce $\mathbf{F} = q(E + \mathbf{v} \times \mathbf{B})$ and, since our inhomogeneous electric field has gradients, is termed the gradient force:

$$F_{grad} = \frac{\alpha}{2}\nabla\langle E^2\rangle, \tag{6.4}$$

$\langle E^2\rangle$ is the time average of the squared electric field vector, which is what the dipole experience, and α is the polarization of the bead and depends on

volume and refractive index:

$$\alpha \propto r^3 \left(\frac{\frac{n_o}{n_s} - 1}{\frac{n_o}{n_s} + 2} \right) \tag{6.5}$$

$\langle E^2 \rangle$ is proportional to the intensity of the laser and the gradient force will thus act restoring in the lateral direction due to the Gaussian intensity profile and in the axial direction due to the beam being focussed by a lens.

The name Rayleigh regime naturally refers to Rayleigh scattering. Incoming light will excite the atoms (and molecules) in the bead, leaving them in a higher energy state that must be abandoned either by absorbtion or scattering. Absorption is the dissipation of added energy in vibrational states i.e. heating, while scattering refers to the remitting of light quants of appropriate energy in arbitrary direction. Scattering events may leave the atom in a slightly energized state and thus also inflict some degree of heating. The ratio of absorption and scattering is dependent on the material i.e accessible energy states and the wavelength of incoming light, however, both phenomena act to push the bead in direction of propagation. Below is the force arising from scattering:

$$\mathbf{F}_{scattering} = n_s \frac{\sigma \langle \mathbf{S} \rangle}{c} \tag{6.6}$$

n_s and the speed of light in vacuum c already familiar quantities. $\langle \mathbf{S} \rangle$ is the time averaged poynting vector of energy flux perhaps better known in the quantity of radiation pressure $\frac{\langle S \rangle}{c}$. σ is the Rayleigh scattering crosssection:

$$\sigma = \frac{8\pi}{3} \left(\frac{2\pi n_s}{\lambda} \right)^4 r^6 \left(\frac{\frac{n_o}{n_s} - 1}{\frac{n_o}{n_s} + 2} \right). \tag{6.7}$$

The force originating from absorption is given in the same manner if one replaces the scattering crosssection with the absorption crossection. The dependence of particle radius for the scattering force is r^6 and it will therefore quickly dominate the gradient force $\propto r^3$ for larger objects and thus make trapping impossible as the object is simply pushed away. For a trapped object the scattering force evidently displaces its center to after the focal point. The scattering force is incorporated into the ray optic description by a more detailed view considering not only transmission but also reflection at the boundaries.

Intermediate region ($d \ll \lambda$)

The two above limiting cases should provide a good understanding of optical trapping. Unfortunately most biological optical trapping experiments are

carried out in the intermediate regime ($d \approx \lambda$), as certain laser wavelengths are desired to minimize absorption and the coherent damage of biological specimens. These wavelengths coincide with the typical size of probes used to handle interesting biological substrates/objects. These handles are most often polystyrene beads with a diameter in the micron range as these are easily observed in the microscope and are excellent subjects for optical trapping. Optical trapping in the intermediate region must be explained by a electromagnetics and Maxwell equations as in the Rayleigh regime. But since the trapped object can no longer be treated as a single point dipole the mathematics become extensive, and is omitted in present text. For a deeper look into optical trapping in the intermediate region see [39].

6.2 The OT setup

A schematic of the used Optical tweezers setup for the series of experiments of this text is depicted in 6.2

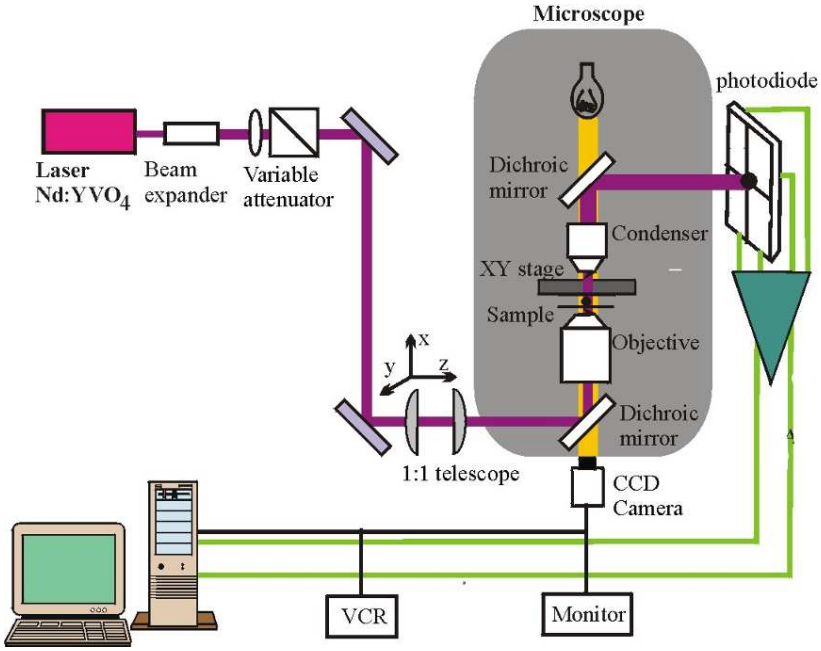

Figure 6.2: A schematic of the overall setup. It does not display the details of DIC. Figure taken from [20].

The optical tweezer setup consists of an inverted light microscope and a

$ND : YVO_4$ 1064nm laser with adjustable power in Tem_{00} mode(Gaussian profile). The movement of a trapped object is recorded by a Position sensitive diode "PSD". The laser beam is expanded to fill the back aperture of the objective and several mirrors direct it properly into the objective where it is then focused by the objective of high numerical aperture to create the axial trapping. The PSD is an array of PIN diodes, it utilizes the photoelectric effect which generates a electric potential from incoming photons, this signal in two components (x, y) is then again multiplied by an electronic amplifier before it is acquired by a NI- Acquisition card and subsequential stored by software(NI Labview). A PSD typically consists of a "high" number of discrete photodiodes, here 256. From the intensity impinging on these individual diodes, it will estimate the center incoming laser/light under the assumption that the incoming light is uniformly distributed, which explains the prefix "position sensitive". The intensity reaching the PSD is related to the scattering from previous section, as light going through the bead will undergo interference and thereby creating a shadow like pattern. The temperature of the sample is maintained by a waterbath stabilized flow trough the sample holder and objective heater. The reason for heating both the objective and sample is to minimize convection. It is necessary to routinely do a calibration of the complete heater setup to insure a appropriate temperature of the sample. The image of the sample is magnified by the same objective that focuses the laser and by a zoom connected to a CCD camera. If one wishes to relate the sample orientation to the PSD signal it can be done by moving the sample with a piezo stage in, e.g. sinusoidal movement, and correlate it to the PSD signal and adjusting the orientation of the latter. This was done. The objective used is a water immersion objective minimizing spherical aberrations. If a an oil or air objective was used such that the light must be travel through additional different media the spherical abbrevations would be larger. The use of a water objective allows measurements throughout the depth of the sample which here is $100\mu m$, and makes both the need to be, and the corresponding theoretical hydrodynamic approximations, for being close to a surface, redundant. In the experiments of this text it is the position detection by the photodiode part of the setup that is central for getting data rather than the image acquisition, and the tweezer functionality is used as control device insuring that beads were properly stuck to the microtubule network.

6.3 DIC

The size of microtubules ($\varnothing \approx 25nm$, $l \approx 1 - 50\mu m$) places it at the lower resolution limit of classical optical microscopy, therefore the technique of differential interference contrast, abbreviated DIC, is applied for better image quality. DIC is on the simplest explanatory level two overlaid bright field images giving a edge contrast with a shadowy or 3D like resemblance. Figure

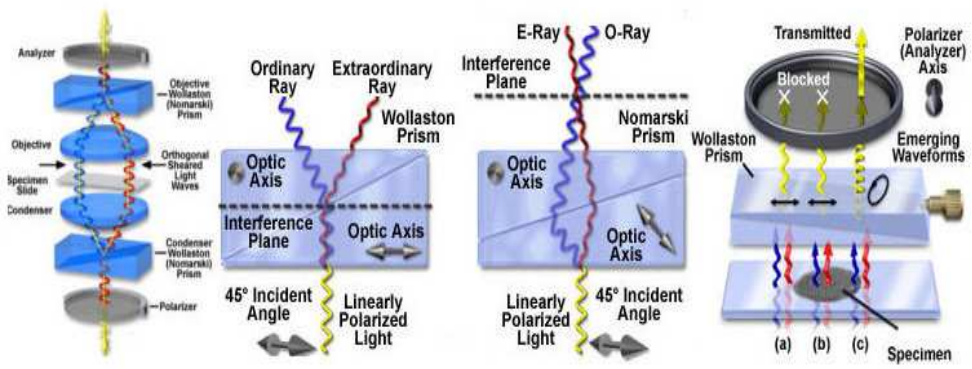

Figure 6.3: The principle behind differential interference contrast. Figure from [21].

6.4 shows the light path and provide additional explanatory illustrations for the light behavior. The lightpath: Coherent light will travel through a polarizing filter and a Normanski prism before arriving at the condenser, and then it will encounter the same two components in reverse succession after the objective. A Normanski prism, which is named after the French inventor of DIC, is a modified Wollaston prism consisting of two quartz wedges as seen in the figure 6.4 left. The first polarizing filter only allows the passage of waves of amplitude vector in one specific direction. The polarized light then enters the Normanski prism, where it at the first boundary is divided into a pair of orthogonal waves (non interfering), these are then sheared (displaced) by a small angle at the edge between the two wedges also known as the inner Normanski boundary. The waves will then after being focused by the condenser travel through the specimen still in close proximity of each other. The second Normanski prism realigns the waves after they have gone through the objective and lets them interfere before exiting. If the pair of orthogonal slightly displaced waves experience a difference in optical path length when traversing the specimen it will induce a phaseshift, giving the wave an elliptic electric field vector(corkscrew), as they are rejoined into a single wave and emerges from the second Normanski prism. For wave pairs that do not experience a difference in their respective optical paths they leave the second

prism with an electric field vector parallel to the one allowed by the first polarizing filter. By a offsetting the two polarizing filters by an 90° angle, only phaseshifted light is allowed to propagate, see figure 6.4 far right. This typically gives a uniform dark background, where areas with great thickness or refractive index gradients appear very bright or dark depending on constructive or destructive interference. For optimal contrast the condenser side alterations must be exactly matched on the objective side as readily seen as a requirement for maximum exclusion of non phaseshifted background light, this is obtained by Kohler illuminating. The shadow quality or "3D" effect of DIC images originates from the wedge shape of the Normanski prisms and the resulting different initial phaseshifts for light across the prism.

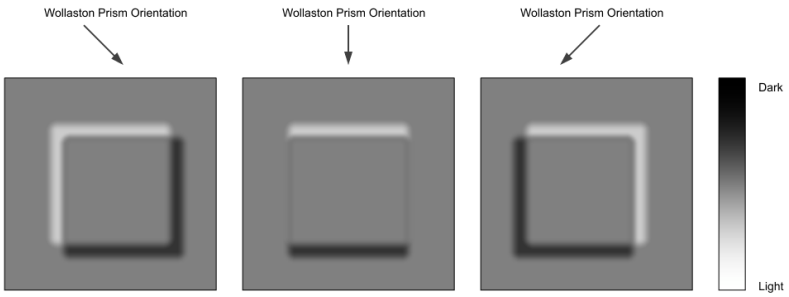

Figure 6.4: DIC images of a square with different orientation of the normanski prism. The images show how the shadowing effect originates from the prism. Figure taken [21].

In practical use the best image is obtained by tinkering with the position of one of the Normanski prism and/or reorientation of the polarizing filters as the quality depends not only on the mutual orientation of the DIC components but also of that of the specimen. This is especially true for long thin objects such as microtubules. One should of course be aware that the contrast is obtained on the basis of optical paths and therefore offers no distinction between refractive or thickness gradients, and combinations these two types.

Chapter 7

Results

A few further observations on the formation of microtubules network in the presence of TPPP/P25, as directly observed by DIC microscopy. The samples were prepared by creating a small tunnel between two coverslides (thickness no. 1) by application of two pieces of double sticky tape. A polymerization solution as in section 4.2 with an appropriate volume of prepared beads, see appendix, was inclosed in the tunnel and a chamber realized by sealing of the ends with either candle wax or silicone. The sample chamber was then mounted at the microscope setup where it was kept at a constant temperature $T \approx 37°C$.

- The overall polymerization seemed to be discrete as either a complete network or nothing would form. It was ergo not possible to observe free individual microtubules when the polymerization process was with TPPP/p25.
- In the initial phase small asters or hubs would form and number and the length of microtubules originating from these would increase with time.
- The formed network would reach a static state after a shorter time period, typically within minutes.
- After a prolonged timeperiod $> hrs$ the network would dissolve rather rapidly as the individual microtubules would disintegrate. In the resulting in a solution full of debris.
- The microtubules of the network would often be curved, and appear in some extend to be crosslinked.

An appropriate bead for measurement was selected on following criteria:

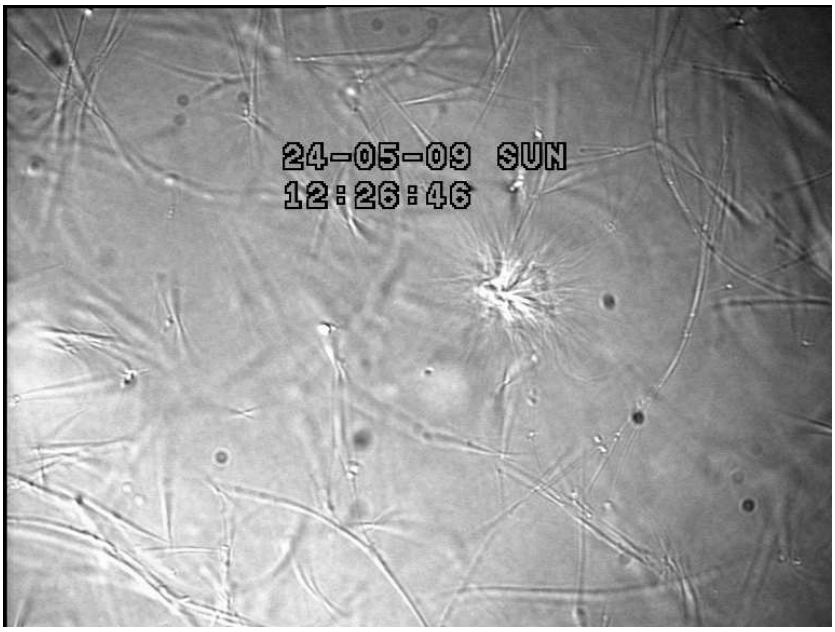

Figure 7.1: DIC pictures of microtubule network formed with TPPP/p25. Notice the curvedness of the microtubules/bundled microtubules and the aster centrosome-like hub in the middle.

- The microtubule or microtubule bundle should be as isolated and in as simple configuration as possible. The tracer bead be placed far from hubs, junctions or crosslinks and the microtubule preferably as straight and long as possible.

- The bead should only be attached to one microtubule. The attachment was tested by pulling with the optical trap temperable deforming the network, and only beads firmly attached used.

- The bead-microtubule complex being a fair distance from the chamber surfaces $d > 10\mu m$, to avoid anomalies related to fluid dynamics near a a surface.

- No free beads or debris in the immediate vicinity such that that the signal would not be disturbed by trapping of such additional material.

The trap and bead were then carefully centered as best as possible, in an iterate process of positioning and applying or canceling the optical trap. This was done to insure a minimal if any tension/stress in the microtubule/network originating from the trap. The $x-$ and $y-$ signal of the photodiode were then recorded in a measurement of 3 seconds sampled at a frequency of $22kHz$,

and such measurements repeated.

Anisotropy

To test for anisotropy the aligned image of the CCD-camera and the photodiode signal were aligned with the orientation of suitable microtubule in respect to a longitudinal and a transverse direction. This was done by reorientation of the sample, such that the microtubule was located along the x or y axis of the photodiode. A such orientation is in its nature based on a local observation and is as such only possible since the microtubules appear rigid. For the microtubules used in this part, such as the one presented in figure 7.2, a such directional determination, however, seems reasonable.

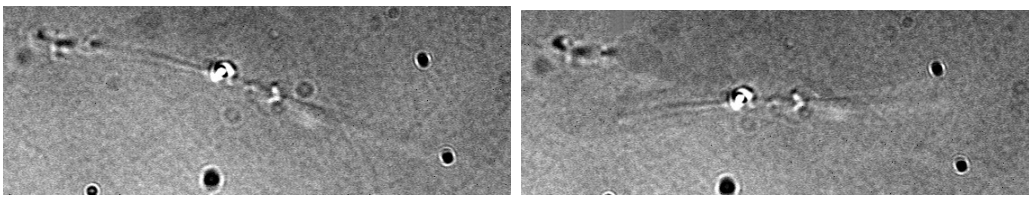

Figure 7.2: DIC images of a microtubule/bundle measured in the series to test for anisotropy, partially out of focus. *Left* Before alignment. *Right* after alignment (sample rotation). The axis of the image were beforehand aligned with the axis of the photodiode. The bead is in the center, to the right of it an anomaly or dirt/debris is attached. Black spots are dirt in the setup and not in the sample.

Figure 7.3 displays the time averaged mean squared displacement of the longitudinal and transverse, x and y, position together with the combined 2 dimensional $r = \sqrt{x^2 + y^2}$ mean squared displacement

$$\langle r(\tau)^2 \rangle = \langle (r(\tau + t) - r(t))^2 \rangle \propto t^\alpha$$

in a double-logarithmic plot, each point MSD(τ)is averaged over $6 \cdot 10^3$ displacements. The data presented in the figures is of one specific measurement, but representative of the general observations.
A number of observations can be made. It is evident, that the overall shape of the mean squared displacement for the two directions are similar. For the smallest timescales from $5 \cdot 10^{-5} s$ to approximately $4 - 5 \cdot 10^{-3} s$ it is a smooth rather rapidly increasing value. For the longer timescales the mean squared displacement is seen to approach an asymptotic value. It is also clear that the amplitude of the two directions are different.

If we look at the corresponding power spectrum density in figure 7.4 *bottom*, we see the points lying nicely on a straight line. It is clearly distinct from

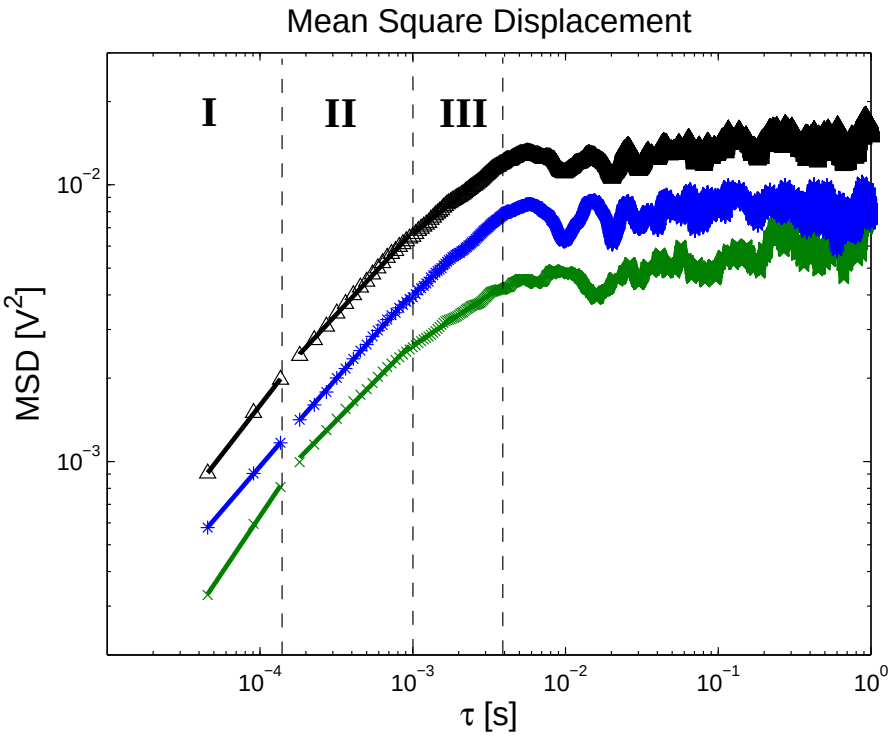

Figure 7.3: The mean square displacements of an 'aligned' microtubule for anisotropy examination. Green cross x-longitudinal along the microtubules. Blue stars y-transverse perpendicular to the microtubules. Black triangle $r(x, y)$. Full lines are fits. The value of each datapoint is based upon $6 \cdot 10^3$ displacements.

the PSD of a freely diffusing bead as seen in figure 7.4 *top*. The PSD of the free bead display a behavior dependent on frequency as described by equation 5.20. The power spectrum density in the presented form is smoothed/binned to give a clearer curve. A corner frequency at lowest frequency would be incorporated into the first bin, which anyway is omitted for the fitting procedure. It should therefore be reasonable to fit the power spectrum density to a power law and extract the scaling coefficient α according to equation 5.19:

$$\langle \tilde{x}(\omega)^2 \rangle \propto \frac{1}{\omega^{1+\alpha}}$$

The PSD was fitted by the method of unconstrained nonlinear minimization of the sum of squared residuals [15] in the interval

$$[300Hz; 5.5 \cdot 10^3 Hz].$$

The upper boundary chosen to satisfy $\omega^2 \ll \omega_{nyquist} = \omega_{sample}/2$, where a Lorentzian is expected to describe data and omits any high-frequency

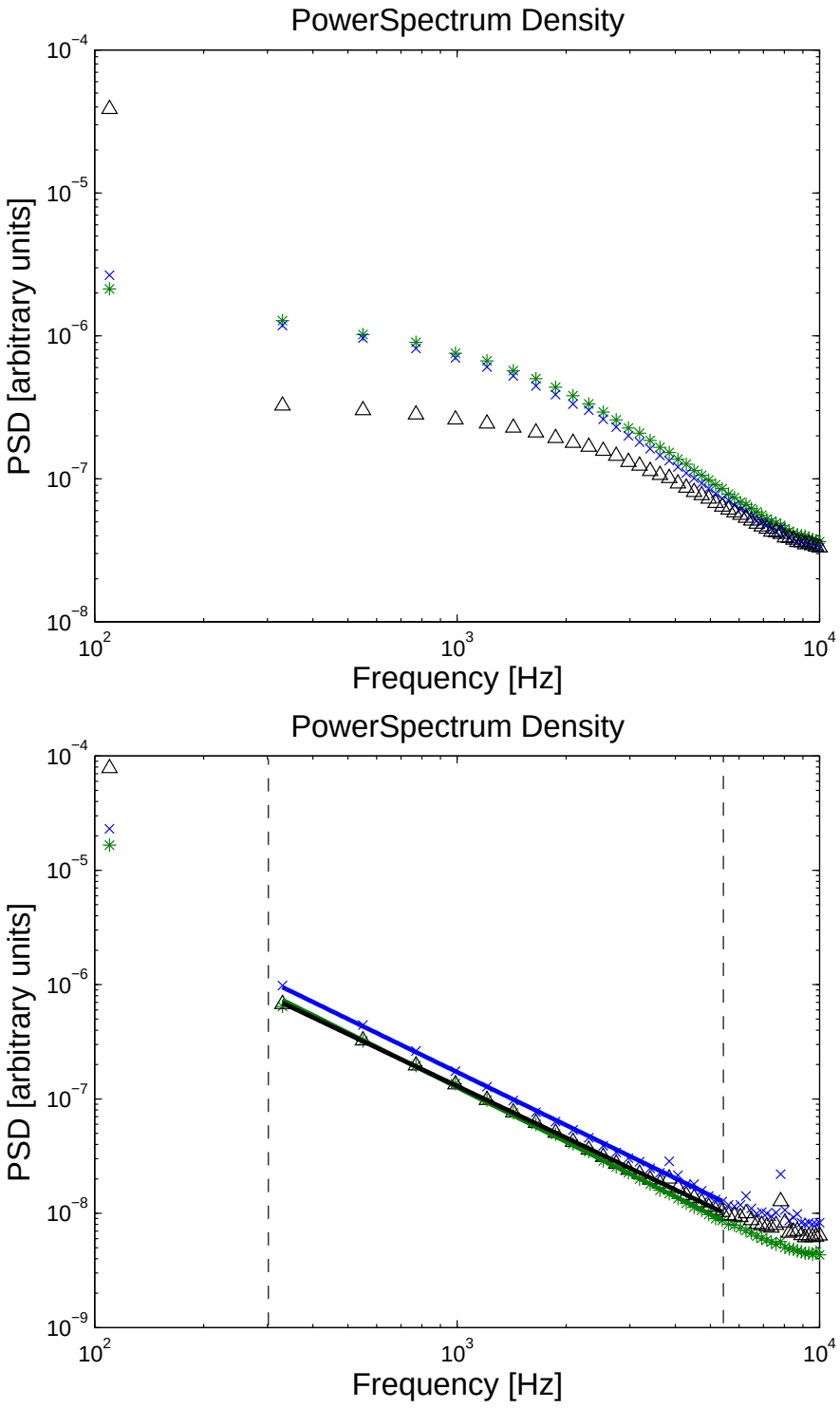

Figure 7.4: Power spectrum densities have been smoothed/binned and as a consequence the first and last point should be disregarded. *top:* PSD of a freely diffusion bead. The behavior is clearly distinct for low and high frequencies. *bottom* Power spectrum density of the measured bead attached to a microtubule network from figure 7.3. Blue represents the transverse y and green the longitudinal x direction. An observation is that the PSD of the r-signal in every case nearly collapses upon the those of the x and y direction for networks measurements, this is not necessarily the case for the PSD of free beads, as seen above.

noise. The mean squared displacement was likewise fitted to a power law by the same method of minimization but in three different intervals of short timescales,

$$\langle \Delta r^2 \rangle \propto \tau^{\alpha}$$

and the exponent α extracted. The three intervals were chosen as to properly include the whole range of short timescales the mean squared displacement rapidly increases. A difference of scaling exponent evaluated on different timescales might be expected as the transition from some diffusive behavior to the plateau of a confined movement, need not and will not, be clear cut, although according to the solutions of Caspi et al. in chapter 5 a transition time can be pinpointed.

$$\begin{aligned} I &: \tau \in [4.5 \cdot 10^{-4}s; 1.4 \cdot 10^{-4}s], \\ II &: \tau \in [1.4 \cdot 10^{-4}s; 10^{-3}s], \\ III &: \tau \in [10^{-3}s; 4 \cdot 10^{-3}s], \end{aligned}$$

Please notice the first interval I only represents the mean squared displacement of very few timelags. As such the fit in this interval cannot be used for validation of model predicting a power law relation. The intervals is indicated in figure 7.3, where the mean squared displacement for each timelag is are averaged over $6 \cdot 10^3$ displacements.

For all measurements, where the mean squared displacement as a function of the timelag has been fitted and the diffusion coefficient α determined, the MSD for each timelag τ is averaged over $65 \cdot 10^3$ displacements. The maximum number of displacements is of course limited by the overall number of positions obtained and the maximum timelags of interest. All fits were in good agreement with the data, with the precaution mentioned for the interval of smallest timescale.

Table 7.1 display the obtained scaling coefficients from both the power spectrum densities and the mean squared displacements in respect to their directional orientation and interval. The mean and standard deviations can be found in 7.2. The p-values of table 7.3 represent the likelihood of an observed difference between the two exponents of the longitudinal and transverse directions to be random according to a Student t-test. A limit for significance is often chosen to be $< 1\%$ depending on preference. None of the values of the experiments indicates any significance. We can therefore conclude that the data show no evidence of anisotropy. For the remainder of measurement no consideration to the directional orientation was thus taken.

If the measurement had shown signs of anisotropy it could mean that we saw the behavior of a single or bundle of microtubule rather than that of a polymer network. If the scaling exponent had been found in proximity

MT	PSD α_{PSD}	PSD α_{PSD}	MSD α_I			MSD α_{II}			MSD α_{III}		
	t	l	t	l	r	t	l	r	t	l	r
A	0.45	0.48	0.60	0.74	0.71	0.46	0.63	0.53	0.43	0.49	0.46
B	0.69	0.58	0.84	0.57	0.63	0.73	0.62	0.65	0.51	0.51	0.51
C	0.27	0.25	0.20	0.56	0.37	0.36	0.42	0.39	0.51	0.68	0.51
D	0.42	0.57	0.58	0.64	0.63	0.56	0.58	0.57	0.48	0.46	0.46

Table 7.1: Table of obtained values of the scaling coefficient α for 4 microtubules with respect to filament orientation by means of the power spectrum density PSD and the mean square displacement MSD. Transverse is indicated by t and the longitudinal direction by l.

	PSD α_{PSD}	PSD α_{PSD}	MSD α_I			MSD α_{II}			MSD α_{III}		
	t	l	t	l	r	t	l	r	t	l	r
mean	0.46	0.47	0.55	0.62	0.57	0.52	0.56	0.54	0.48	0.53	0.49
std. dev	0.17	0.15	0.13	0.08	0.14	0.14	0.10	0.11	0.04	0.03	0.10

Table 7.2: Mean and standard deviation of the found scaling coefficients of table 7.1

	α_{PSD}	α_I	α_{II}	α_{III}
P-value	0.83	0.63	0.47	0.8

Table 7.3: The significance between the found scaling coefficients from the longitudinal an transverse direction was tested according to a Student's t-test within each interval and method. There is no sign of any directional dependency.

of $\alpha \approx 0.75$, it would mean that the persistence length could have been estimated on bases of equation 5.14 and equation 5.16 of chapter 5. Now since such an anisotropy of the scaling coefficient was not observed, we can also with a reasonable certainty state that the movement of a bead represents the movement and properties of the network as a whole. Beads identified as freely diffusing were tested according to equation 5.20, to validate if they indeed were so; just to remind for the beads to comply with the relation 5.20 their diffusion coefficient must be one, $\alpha = 1$. There was a very good agreement between the observed movement of the free beads and the expected. Had these beads showed a behavior identical to those of table 7.1 i.e. subdiffusive, it would have indicated a composition of the polymer network smaller, than what was possible to resolve directly by DIC imaging. This would also have rejected a need to define orientation. The good agreement also served to insure that the setup otherwise was functioning as expected, and of course provide the control.

The observation of different amplitudes of the mean square displacement for large timescales of the longitudinal and transverse direction of individual measurements is not in conflict with the notion of a discrete network. A bead attached to one microtubule would have a larger freedom to move in the transverse direction than that of the longitudinal, since movement in the latter would require the deformation of several microtubules.

7.1 Scaling coefficient

Since there was no sign of anisotropy the criteria for microtubule attached beads to be chosen could be adjusted and allow for a wider selection among the limited number. In figure 7.5 the mean square displacements of one measurement of all the measured beads is shown. The MSD(τ) is in this figure averaged over only 10^3 displacements per lag time. For all of them we see the same overall shape as previously described. The corresponding scaling coefficients for the same recorded measurements is seen in table 7.4. Again for fitting procedures the MSD of each timelag τ is averaged over $63 \cdot 10^3$ displacements. Fitting method and intervals I,II, and III as introduced in previous section. The standard deviation is obtained from several 3 seconds measurements on the same microtubule attached bead. For each of these measurements the MSD has been calculated and fitted to find α, and the standard deviation presented here is he deviation of these α's. Again all fits where in general in a reasonable agreement with the data.

We see from table 7.5 that the mean of the scaling coefficient α from the power law fitting of the MSD is similar for the 3 intervals. But the table also

	PSD	MSD		
MT	$\alpha_{PSD} + std.dev.$	$\alpha_I + std.dev.$	$\alpha_{II} + std.dev.$	$\alpha_{III} + std.dev.$
1	0.56 ± 0.032	0.63 ± 0.043	0.57 ± 0.032	0.46 ± 0.034
2	0.47 ± 0.053	0,52 ± 0.037	0.76 ± 0.058	0.62 ± 0.048
3	0.38 ± 0.021	0.65 ± 0.033	0.53 ± 0.025	0.45 ± 0.027
4	0.38 ± 0.018	0.33 ± 0.029	0.56 ± 0.021	0.70 ± 0.025
5	0.60 ± 0.048	0.34 ± 0.056	0.62 ± 0.049	0.56 ± 0.043
6	0.67 ± 0.037	0.64 ± 0.029	0.66 ± 0.034	0.50 ± 0.051
7	0.44 ± 0.023	0.72 ± 0.022	0.56 ± 0.016	0.43 ± 0.017
8	0.48	0.75	0.59	0.56
9	0.34 ± 0.033	0.64 ± 0.030	0.51 ± 0.027	0.71 ± 0.025
10	0.23 ± 0.032	0.42 ± 0.037	0.65 ± 0.036	0.27 ± 0.034
12	0.19 ± 0.036	0.20 ± 0.040	0.37 ± 0.042	0.36 ± 0.033
13	0.24 ± 0.025	0.41 ± 0.044	0.40 ± 0.038	0.67 ± 0.037
14	0.59 ± 0.019	0.59 ± 0.027	0.63 ± 0.026	0.55 ± 0.031

Table 7.4: Obtained values of the scaling coefficient α from the power spectrum density and the mean square displacement. The standard deviation is given when the specific bead has been measured more than once, and based upon coefficients fitted for each measurement. There was only one measurement of microtubule attached bead 8, additional was data corrupted.

	PSD	MSD		
	α_{PSD}	α_I	α_{II}	α_{III}
mean	0.42	0.52	0.57	0.52
std. dev.	0.15	0.17	0.1	0.13

Table 7.5: Mean and standard deviation of the scaling coefficient α from the power spectrum density and the mean square displacement of table 7.4

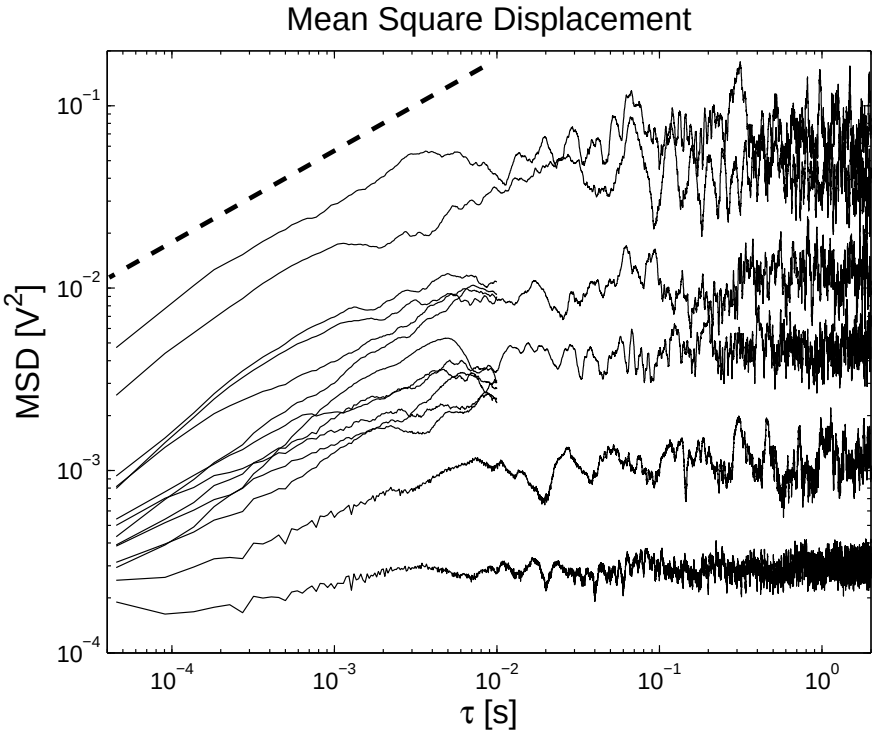

Figure 7.5: The mean square displacements measured from the networks, each datapoint based on 10^3 obtained positions. Not all MSD(τ) are plotted for full timelag to avoid cluttering at the high timescales, ones displayed representative are of all. Dashed line represent a slope of $\alpha = 1/2$.

reveal that the standard deviation of the obtained values is rather large. To test for any significant difference between the scaling coefficient of the three intervals and the PSD analysis a Student's t-test was done, see table 7.6. There is no indication of any significant difference. The smallest likelihood $p \approx 1\%$ is found between the mean squared displacement obtained in interval II and the values obtained from the power spectrum. It is however, not small enough to validate a significant difference in present text.

Reviewing figure 7.5 it is evident, that the amplitude of the constant plateau for large timelags does vary between the different measurements. For measurements on the same bead the plateau values are overlapping, not shown. The data is not conclusive to whether or not a relation between the final plateau amplitude and scaling coefficient exist. Since the number of measured microtubule attached bead is rather limited (14) they are not associated with their network in the presentation here (junk information), and does not display any tendency for values to be dependent on this.

Oscillations:

	α_{PSD}	α_I	α_{II}	α_{III}
α_{PSD}	-	0.15	0.01	0.09
α_I	0.15	-	0.46	0.94
α_{II}	0.01	0.46	-	0.35
α_{III}	0.09	0.94	0.35	-

Table 7.6: Probability of randomness according to a Student's t-test

If, we are satisfied with describing the mean squared displacement as a function of timelag by an initial increasing value approaching a asymptotic value or plateau, we can normalize each MSD(τ) series by evaluating the constant value $MSD(\infty)$, which is approached as $\tau \to \infty$. This value $MSD(\infty)$ was averaged in the interval $\tau \in [10^{-1}]; 1s]$, and a few such normalized of network MSD's together with that of a free bead, can be seen in figure 7.6. The normalized MSD are averaged on basis of $42 \cdot 10^{-3}$ displacements rather than the few thousands of figure 7.5. The figure clearly shows oscillations of the MSD(τ), and they seem to be in sync. The free bead does not experience oscillations, at least not comparable to those of the bead attached to microtubules. Two of the measured microtubule attached beads, not shown, does not show these large oscillations but are still distinct from the free bead, in terms of the timescale of their initial increase. The reason is unknown. Looking at figure 7.7, where the normalized MSD(τ) plotted for a larger time range but have maintained a large number of displacements to average over pr timelag is plotted. It is evident, that the amplitude of the oscillations decrease with growing time lag τ. This is common for all the measured beads displaying the oscillations. Figure 7.6 and figure 7.7 also reveal one more information: the saturated $MSD(\infty)$ is not reached at the interval used to determine MSD(∞). The normalized mean of the oscillation clearly is not unity for the smaller timelags i.e. we have something truly resembling a asymptotic behavior. Where the final plateau is not reached until larger timescales.

The reason for not plotting the MSD(τ) traces with maximum precision from the beginning was simply to avoid that their oscillatory behavior would steal all attention.

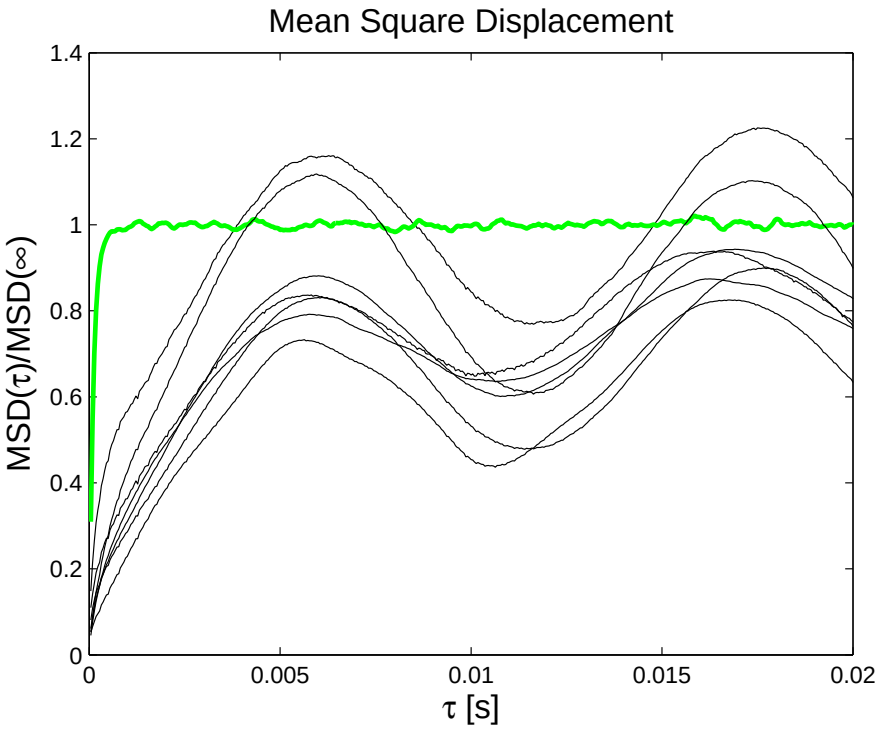

Figure 7.6: Selected, but representative, normalized mean square displacement. Black network measurements. Green free bead. The networks measurements clearly exhibit an oscillating behavior, that is not evident for the freely diffusion bead. MSD(τ) averaged over $42 \cdot 10^{-3}$.

7.2 Discussion

The experiments showed no signs of anisotropy, and it is therefore clear, that they must represent the bulk properties of a network. However, that the individual measurements have different amplitudes or maximum defections $MSD(\infty)$, indicates some degree of heterogenesis or discreteness in the microtubules networks. The overall shape of the MSD(τ) was in agreement with what was expected: With an upper limit of the MSD(τ), as the bead would be confined by either the network or the optical trap and an initial rapidly increasing MSD(τ) was also predicted as a polymer solution is not expected to be purely elastic. That no anisotropy was discovered is perhaps somewhat more surprising given the otherwise discrete appearance of the network.

The relatively large spread of α-values within the intervals of timelag chosen for evaluation of the MSD(τ) seems to support an assumption of a the network being inhomogeneous. microtubules in a inhomogeneous network must experience different entanglements and as a consequence have their

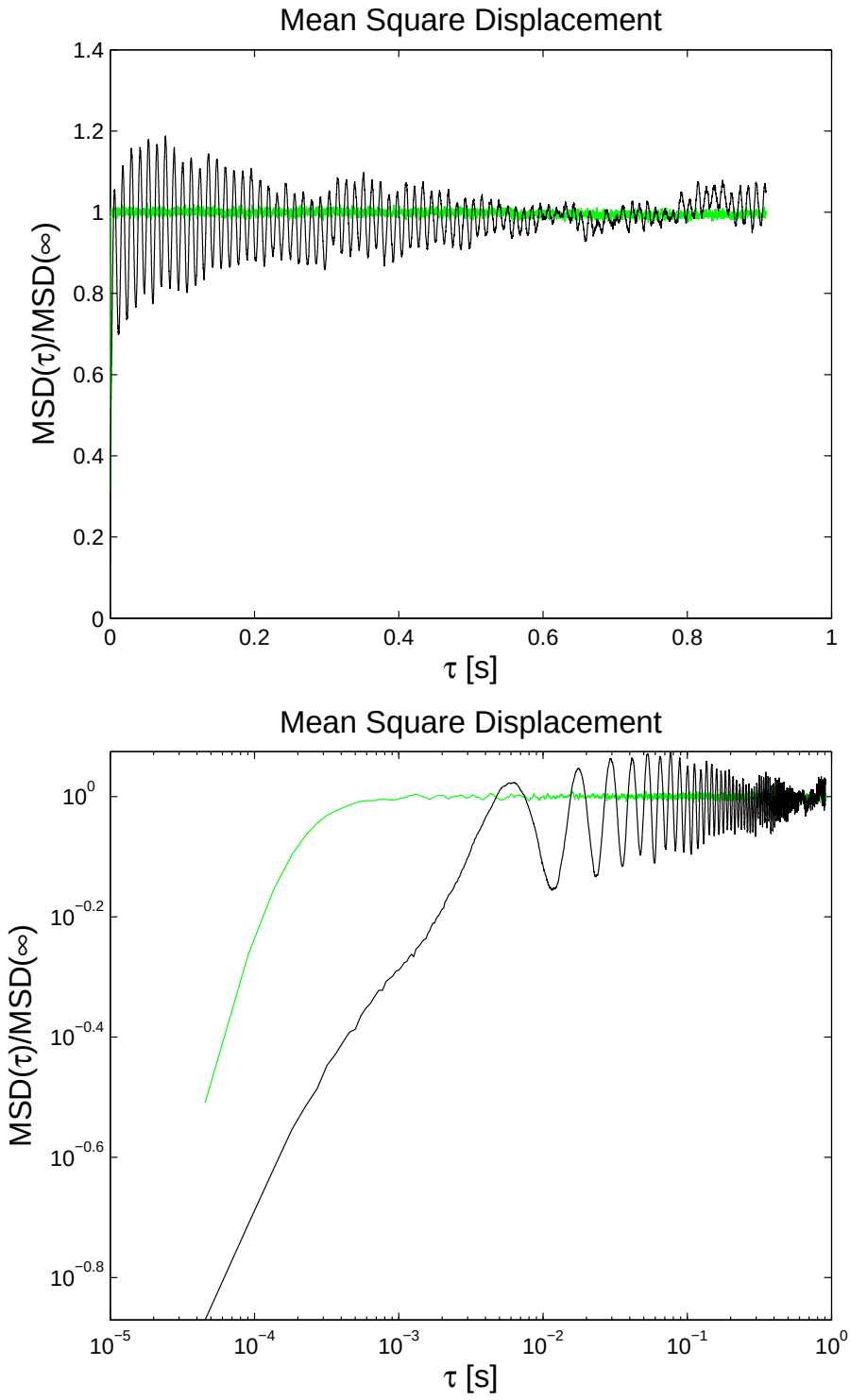

Figure 7.7: *top:* Normalized MSD linear plot *bottom* Normalized MSD double logarithmic plot. Black network measurement. Green freely diffusing bead. The amplitude of the oscillating network MSD clearly diminishes with growing timestep τ.

movement restricted in different degree. The values of the scaling coefficient determined on the background of analysis of the mean squared displacements showed no significant difference between the intervals. Giving the large spread the number of different microtubule attached beads that are measured, apparently needs to be larger to disclose such a difference.

If we look at the coefficient α extracted from the three intervals of the MSD(τ) and from the power spectrum densities in table 7.5, it is clear, even with their large standard deviation, that the value is closer to a value of $\alpha \approx 0.5$ than to the theoretically expected $\alpha = 0.75$, see equation 5.14. This theoretical value have been experimental documented for granules in living yeast cells: [44] $\alpha \approx 0.74$ for timescales $[10^{-5}; 10^{-3}]$s, for *in vitro* actin networks in [1] $\alpha \approx 0.73$ and [16] $\alpha \approx 0.76$, and finally *in vitro* for dynamic microtubules in [7] $\alpha \approx 0.75$.

Scaling coefficients of $\alpha = 0.5$ have previously been reported by microrheological experiments among others on polyethylene oxide (PEO) polymer solutions [41], but only for timescales below $10^{-4}s$. In general such chemical or syntectic polymers are probably too soft to be reviewed as semiflexible, and therefore one cannot expect similar behavior.

Instead we turn once again to Caspi et. al [7], where such a lower coefficient also was seen for microtubules. Their experiments observed the transverse mean squared displacement of microtubules by attached beads using image analysis. Their microtubules were the regular dynamic types and hence more straight than curved. By letting the microtubules polymerize outside the sample chamber and thereby allow them to grow longer than the chamber dimensions, tension would arise as they were flushed into the chamber. Measurements on these stressed microtubules gave exponents $\alpha \in [0.4; 0.5]$. They present the following theoretical relation for a limited range

$$\langle \Delta y^2(x, \tau) \propto \frac{K_B T}{(\sigma\eta)^{1/2}} \tau^{1/2}, \tag{7.1}$$

where σ is the tension along the microtubule.

The microtubules in the experiments of this text were grown inside the sample chamber, and hence no artificial tension should be introduced. Reviewed in the context of the above introduction of tension the lower scaling coefficient of the present experiments seems to be consistent with the curved nature of the microtubules here. It implies that TPPP/P25 is behind the deviance of the diffusion coefficient.

When the MSD(τ) of the measurements are averaged over several thousand displacements, we clearly see the oscillatory behavior expected from the analytical solution of section 5.1.

Regarding the choice of 3 seconds measurements sampling at $22kHZ$ is is a rather arbitrary choice. The largest timelag used for the fitting procedure is $4 \cdot 10^{-3}$s and the values of determined α's almost are identical when first the MSD(τ) is averaged over 10k+ displacements, the measurements could have been split up into several measurements instead, to try to minimize the standard deviation (rounding of the numbers). But as, albeit arbitrary, choice the standard of 3 seconds stands. The choice of the fitting intervals I,II and III apart for covering the full timescale of the initial rapid increase is also arbitrary and the timerange could be split up in even more or different intervals.

Chapter 8

Conclusion

The project rather presents a range of qualitative description rather than neat quantitatively discoveries.

The experimental estimation of the persistence length of microtubules as originally desired was never successful, as it was halted by the inability to produce solutions of individual microtubules.

During the process to polymerize such solutions of individual microtubules, inadvertently the contents of [14] and partially [9] on the formation of taxol crystals was reproduced. Taxol asters and needlelike crystals with or without the presence of tubulin were documented by DIC and electron microscopy. The reason of failure to produce single individual microtubules either as taxol- or GMPCPP- stabilized, or as regular dynamic microtubules, remain undisclosed. It is especially perplexing, that a protocol devised and followed with success in Amsterdam could not be reproduced in Copenhagen. There are no other reasons to suspect e.g. a pollutant at the NBI, and it would also be difficult to imagine such a factor capable to effectively hinder tubulin polymerization under the variety of polymerization conditions followed. The best guess is perhaps faulty tubulin, al tough this was replaced on several occasions.

However, large *in vitro* networks of microtubules polymerized in the presence of TPPP/p25 were created, and microrheological experiments conducted on these. The mean squared displacement as a function of lagtime showed for the microtubule attached beads, a qualitatively agreement with the recent analytical solution by Desposito and Vinales 2009 [11] for a bead embedded in a viscoelastic polymer network and under the influence of a harmonic potential, section 5.1. There were no direct quantified comparison of this analytical solution and the experimental found values done this project.

The subdiffusive behavior of these networks was evaluated in respect to the coefficient of diffusion for small timelags $[4.5 \cdot 10^{-4}s; 4 \cdot 10^{-3}s]$ by fitting a

power law to the MSD(τ), and by fitting a power law to the power spectrum density of the timeseries of the photodiode. Both methods provided diffusion constants α without any significant difference. The values revealed a rather large spread, but it seems clear, that they remain below an expected value of $\alpha = 0.75$ found experimentally for other polymer networks. Their means were found to be 0.42 ± 0.15 and 0.52 ± 0.17, 0.57 ± 0.10 0.52 ± 0.13 for the PDS analysis and the three intervals of the MSD analysis, respectively. The deviance seems to be a consequence of TPPP/p25 as the networks would have centrosome-like hubs and curved microtubules. It can de facto not be stated, as no control experiments on regular microtubules solutions could be done.

The overall improvement of this project would be the ability to polymerize microtubules without TPPP/P25, preferable in solution of individual microtubules. The motivations in chapter 3 for determining the persistence length on basis of cantilevered individual microtubules still remain.

In respect to the microrheological experiments with TPPP/p25 polymerized microtubules networks done in present text, it would be nice to obtain more measurements. The work here only have measurements of 14 different microtubules attached beads. Provided a supply of TPPP/p25, it should be straightforward to produce more measurements. Possible a increased number of measurements would allow a better resolution of the MSD(τ) on smaller timescales, and the measurements might advantageously be done at a even higher sampling frequency.

Providing the ability to create a solutions of individual regular dynamic microtubules, it would first serve as a control to the measurements on TPPP/p25 networks, but it then might be interesting to see the behavior of such regular microtubules solutions when adding TPPP/p25 at increasing concentrations. The effect of TPPP/p25 upon already polymerized microtubules could be a valuable information. In the context of the lower scaling $\alpha < 0.75$ coefficient being interpreted as sign of stress in the microtubule: If regular microtubules would have a decreasing coefficient α, when TPPP/p25 is added without hubs forming it would mean that TPPP/p25 bends microtubules/eschew their lattice. If not, the found scaling in TPPP/p25 polymerized networks here, would be a consequence of them originating from the centrosome-like hubs. Whether or not it should be interpreted as tension is debatable.

Chapter 9

appendix

9.1 A: Bead preparation

To make tracer particles, i.e polysterene bead, bind to microtubules the following protocol of bead preparation as successful, most of the time. This protocol differs from most litterateurs where neutravidin or streptavidin coated beads are used and thus require a certain percentage of used tubulin to be biotinylated. The used beads were PC-CAHL-0.8 lot. GKV01: anti-Mouse Immunoglobulin G produced in Goats, coated polystyrene beads of size $0.7 - 0.9\mu m$ from Kisker. To provide the link between the igG and tubulin the beads need an additional coating of Anti-β-Tubulin II antibody produced in mouse, Sigma. Steps as follows.

- $50\mu L$ Original beads diluted in 500 μL water.
- Spin for 12 min at $\approx$ 4000rpm, keep acceleration below 1000G. Remove supernatant and refill with water to $550\mu L$. Repeat this for 3 cycles
- Resuspend in $50\mu L$ BRB80
- Sonicate for 30- 60sec and check the degree of stickiness and repeat until acceptable or start over.
- Add $1.5\mu L$ Anti-β-Tubulin II antibody, mix for at least 1 hour.
- Spin for 12 min at $\approx$ 4000rpm, remove supernatant and refill with BRB80 to $550\mu L$. Repeat this for 3 cycles
- Resuspend in $50\mu L$ BRB80

The beads if properly prepared will usually last for a period of some days, but will eventually either stick or lose functionality. Sonication after the addition of the tubulin antibody is not recommended, if necessary try a small volume and dilute plenty.

9.2 B: EM staining

The following procedure was after some tweaking found to be efficient for negative staining of microtubules to be viewed in an electron microscope. It is negative staining with heavy atoms. The grids should be 200 mesh copper or similar, but must be formvar -carbon coated. A solution of the stain, uranyl-acetat of $\approx 4\% w/V$ that will probably not dissolve completely should be prepared and stored dark and cold (fridge). A sample of microtubules is prepared as desired, and diluted as appropriate. On a piece of paraffin line up the following for each grid and move it grid from top to bottom.

- $3\mu L$ sample -leave on grid for 2 min.
- $20\mu L$ water -quickly dip grid (rinse).
- $20\mu L$ uA solution -quick dip for precipitation.
- $20\mu L$ uA solution -leave for 1-2 min.
- $20\mu L$ water - rinse 20 secs
- $20\mu L$ water - rinse 20 secs
- $20\mu L$ water - rinse 20 secs

Sample ready, should be viewed within a relatively short timeperiod.

Uranyl acetat ($UO_2(CH_3COO)_2 \cdot 2H_2O$) is derived from uran and maintain some degree of radiation allthough at a non hazardous level when not entering the body through ingestion or skin; use gloves.

Glossary

BRB80 Basic tubulin buffer: $80mM\ PIPES$, $1mM\ MgCl2$, $1mM\ EGTA$, PH adjusted to $\approx 6,8$ with KOH

cilia Cilia is Latin for eyelash. These tiny protuberances on single-cells organisms wave-like hairs to move the cell around or something around the cell, powered by hydrolysis of ATP in mitochondria.

DMSO Dimethyl sulfoxide $(CH_3)_2SO$ Colorless liquid is an polar aprotic solvent that dissolves both polar and nonpolar compounds and is miscible in a wide range of organic solvents as well as water. It has a distinctive property of penetrating the skin very readily. Side effects include stomach upset, sensitivity to light, visual disturbances, and headache. Skin irritation can develop at the site where DMSO is applied topically.

flagella *See cilia* Same construction as cilia but typically longer. Flagella of bacteria are apparently powered by a specific F1 placed at their root,

GMPCPP Guanosine-5'-[(α,β)-methyleno]triphosphate $C_{11}H_{15}N_5O_{13}P_3$ molar mass $518,18g/mol$ also known as CpCpp a Non-hydrolyzable GTP analog allowing polymerization of tubulin but preventing depolymerization.

GTP Guanosine-5'-triphosphate $C_{10}H_{16}N_5O_{14}P_3$ a purine nucleotide of molar mass $523.18g/mol$. GTP is involved in energy transfer within the cell. For instance, a GTP molecule is generated by one of the enzymes in the citric acid cycle. Hydrolysis by dephosphorylation $GTP \rightleftharpoons GDP + P_i$

Lamellipodia are a characteristic feature at the front, leading edge, of motile cells. They are believed to be the actual motor which pulls the cell forward during the process of cell migration. It is a polymerizing network/mesh of linked actin filaments and extends the lamella forward and thus advance the cell's front.

MAP's Microtubule associated proteins. This is the common name of proteins that is associated to microtubules/tubulin and is divided into to classes. A large variety of MAPs have been identified in many different cell types, and they have been found to carry out a wide range of functions. These include both stabilizing and destabilizing microtubules, guiding microtubules towards specific cellular locations, cross-linking microtubules and mediating the interactions of microtubules with other proteins in the cell and include MAP1-class typically found in dendrites and axons and class-2 types such as MAP4, tau and Xmap215 (TPPP)

microspikes Within most lamellipodia are ribs of actin called microspikes, which, when they spread beyond the lamellipodium frontier, are called filopodia.

myelin sheath The myelin sheath or medullary sheath is a electric/pressure insulating myelin layer inclosing some axons allowing the transmission of signals at a higher speed than in non myelin sheathed ones. In the central nervous system the sheath is formed by the oligodendrocytes, while it in the periapical is formed by the schwann cells.

Taxol or Paclitaxel $C_{47}H_{51}NO_{14}$, $853,906 g/mol$ N.B. Taxol is toxic; leads to cell death and should be handled with care especially when dissolved in DMSO which is easily permeable through skin and partly through standard latex gloves.

vertebrate The class of animals with a backbones or spinal columns. Insects which constitutes the vast majority of species, bacteria excluded, are not vertebrates

Bibliography

[1] F. Amblard, A. C. Maggs, B. Yurke, A. N. Pargellis, and S. Leibler. Subdiffusion and anomalous local viscoelasticity in actin networks. *Phys. Rev. Lett.*, 77(21):4470–, November 1996.

[2] Howard C. Berg. *Random walks in biology, expanded edition*. Princeton university press, 1993.

[3] Kirstine Berg-Sorensen and Henrik Flyvbjerg. Power spectrum analysis for optical tweezers. *Review of Scientific Instruments*, 75(3):594–612, 2004.

[4] David H. Boal. *Mechanics of the cell*. Cambridge University press, 2002.

[5] Julian Lewis Martin Raff Keith Roberts Peter Walter Bruce Alberts, Alexander Johnson. *Molecular Biology of the Cell - Fifth Edition*. Garland Science - Molecular Biology of the Cell, 2007.

[6] M Caplow and J Shanks. Evidence that a single monolayer tubulin-gtp cap is both necessary and sufficient to stabilize microtubules. *Mol Biol Cell.*, 7(4):663675, 1996.

[7] A. Caspi, M. Elbaum, R. Granek, A. Lachish, and D. Zbaida. Semiflexible polymer network: A view from inside. *Phys. Rev. Lett.*, 80(5):1106–, February 1998.

[8] D. Gard P. T. Tran Cassimeris, L. and H. P. Erickson. 2001. XMAP215 is a long thin molecule that does not increase microtubule stiffness. J. Cell Sci. 114:30253033. [PubMed]. Xmap215 is a long thin molecule that does not increase microtubule stiffness. *J. Cell Sci.*, 114:30253033., 2001.

[9] Javier S. Castro, Bartosz Trzaskowski, Pierre A. Deymier, Jaim Bucay, Ludwik Adamowicz, and James B. Hoying. Binding affinity of fluorochromes and fluorescent proteins to taxol(tm) crystals. *Materials Science and Engineering: C*, 29(5):1609–1615, June 2009.

[10] Cecilia Conde and Alfredo Caceres. Microtubule assembly, organization and dynamics in axons and dendrites. *Nat Rev Neurosci*, 10(5):319–332, May 2009.

[11] M. A. Desposito and A. D. Vinales. Subdiffusive behavior in a trapping potential: Mean square displacement and velocity autocorrelation function. *Physical Review E (Statistical, Nonlinear, and Soft Matter Physics)*, 80(2):021111, 2009.

[12] Ariane Dimitrov, Melanie Quesnoit, Sandrine Moutel, Isabelle Cantaloube, Christian Pous, and Franck Perez. Detection of gtp-tubulin conformation in vivo reveals a role for gtp remnants in microtubule rescues. *Science*, 322(5906):1353–1356, 2008.

[13] R. Frank Felgner, H. and M. Schliwa. Flexural rigidity of microtubules measured with the use of optical tweezers. *J. Cell Sci.*, 109:509516, 1996.

[14] Margit Foss, Buck W. L. Wilcox, G. Bradley Alsop, and Dahong Zhang. Taxol crystals can masquerade as stabilized microtubules. *PLoS ONE*, 3(1):e1476, 01 2008.

[15] Philip E. Gill and Walter Murray. Algorithms for the solution of the nonlinear least-squares problem. *SIAM Journal on Numerical Analysis*, 15(5):977–992, 1978.

[16] F. Gittes, B. Schnurr, P. D. Olmsted, F. C. MacKintosh, and C. F. Schmidt. Microscopic viscoelasticity: Shear moduli of soft materials determined from thermal fluctuations. *Phys. Rev. Lett.*, 79(17):3286–, October 1997.

[17] Claus Heussinger, Mark Bathe, and Erwin Frey. Statistical mechanics of semiflexible bundles of wormlike polymer chains. *Physical Review Letters*, 99(4):048101, 2007.

[18] Emma Hlavanda, Janos Kovacs, Judit Olah, Ferenc Orosz, Katalin F. Medzihradszky, and Judit Ovadi. Brain-specific p25 protein binds to tubulin and microtubules and induces aberrant microtubule assemblies at substoichiometric concentrations. *Biochemistry*, 41(27):8657–8664, July 2002.

[19] Jonathon Howard. Molecular mechanics of cells and tissues. *Cellular and Molecular Bioengineering*, 1(1):24–32, March 2008.

[20] http://www. nbi.dk/ tweezer/.

[21] http://www. olympusmicro.com/.

[22] M. E. Janson and M. Dogterom. A bending mode analysis for growing microtubules: evidence for a velocity-dependent rigidity. *Biophys. J.*, 87:27232736, 2004.

[23] Marcel E. Janson, Mathilde E. de Dood, and Marileen Dogterom. Dynamic instability of microtubules is regulated by force. *J. Cell Biol.*, 161(6):1029–1034, 2003.

[24] Albertas Janulevicius, Jaap van Pelt, and Arjen van Ooyen. Compartment volume influences microtubule dynamic instability: A model study, February 2006.

[25] Daniel Otzen ; D. Lundvig ; Reinhard Wimmer ; L. Hatting ; J. R. Pedersen ; P. H. Jensen. p25 alpha is flexible but natively folded and binds tubulin with oligomeric stoichiometry. *Tidsskriftstitel: Protein Science*, 14:1396–1409, 2005.

[26] c Kenji Kawaguchia, Shinichi Ishiwatab and Toshihide Yamashitaa. Temperature dependence of the flexural rigidity of single microtubules. *Biochemical and Biophysical Research Communications*, 366:637–642, 2007.

[27] Jacob W. J. Kerssemakers, E. Laura Munteanu, Liedewij Laan, Tim L. Noetzel, Marcel E. Janson, and Marileen Dogterom. Assembly dynamics of microtubules at molecular resolution. *Nature*, 442(7103):709–712, August 2006.

[28] Alexey Khodjakov, Lily Copenagle, Michael B. Gordon, Duane A. Compton, and Tarun M. Kapoor. Minus-end capture of preformed kinetochore fibers contributes to spindle morphogenesis. *J. Cell Biol.*, 160(5):671–683, 2003.

[29] Masashi; Tosa Valer; Tashiro Hideo Kikumoto, Mahito; Kurachi. Flexural rigidity of individual microtubules measured by a buckling force with optical traps. *Biophysical Journal*, 90:1687–1696, 2006.

[30] J. C. Kurz and Jr. R. C. Williams. Microtubule-associated proteins and the flexibility of microtubules. *Biochemistry*, 34:1337413380, 1995.

[31] Atilla Lehotzky, Laszlo Tirian, Natalia Tokesi, Peter Lenart, Balint Szabo, Janos Kovacs, and Judit Ovadi. Dynamic targeting of microtubules by tppp/p25 affects cell survival. *J Cell Sci*, 117(25):6249–6259, 2004.

[32] Helder Maiato, Jennifer DeLuca, E. D. Salmon, and William C. Earnshaw. The dynamic kinetochore-microtubule interface. *J Cell Sci*, 117(23):5461–5477, 2004.

[33] Hideo Tashiro Masashi Kurachi, Masayuki Hoshi. Buckling of a single microtubule by optical trapping forces: Direct measurement of microtubule rigidity. *Cell Motility and the Cytoskeleton*, 30:221–228, 1995.

[34] T. G. Mason, K. Ganesan, J. H. van Zanten, D. Wirtz, and S. C. Kuo. Particle tracking microrheology of complex fluids. *Phys. Rev. Lett.*, 79(17):3282–, October 1997.

[35] B. Mickey and J. Howard. 1995. Rigidity of microtubules is increased by stabilizing agents. J. Cell Biol. 130:909917. [PubMed]. Rigidity of microtubules is increased by stabilizing agents. *J. Cell Biol.*, 130:909–917, 1995.

[36] F. Orosz and J. Ova di. Tppp orthologs are ciliary proteins. *FEBS Lett*, 582:2008. 582:, 2008.

[37] Francesco Pampaloni and Ernst-Ludwig Florin. Microtubule architecture: inspiration for novel carbon nanotube-based biomimetic materials, June 2008.

[38] Francesco Pampaloni, Gianluca Lattanzi, Alexandr Jon, Thomas Surrey, Erwin Frey, and Ernst-Ludwig Florin. Thermal fluctuations of grafted microtubules provide evidence of a length-dependent persistence length. *Proceedings of the National Academy of Sciences*, 103(27):10248–10253, 2006.

[39] Alexander Rohrbach. Stiffness of optical traps: Quantitative agreement between experiment and electromagnetic theory. *Phys. Rev. Lett.*, 95(16):168102–, October 2005.

[40] Christine Selhuber-Unkel, Pernille Yde, Kirstine Berg-Sorensen, and Lene B. Oddershede. Variety in intracellular diffusion during the cell cycle. *Physical Biology*, 6(2):025015–, 2009.

[41] Joris Sprakel, Jasper van der Gucht, Martien A. Cohen Stuart, and Nicolaas A. M. Besseling. Brownian particles in transient polymer networks. *Phys. Rev. E*, 77(6):061502–, June 2008.

[42] Katja M. Taute, Francesco Pampaloni, Erwin Frey, and Ernst-Ludwig Florin. Microtubule dynamics depart from wormlike chain model. *Physical Review Letters*, 100:028102, 2008.

[43] L. Tirin, E. Hlavanda, J. Olh, I. Horvth, F. Orosz, B. Szab, J. Kovcs, J. Szabad, and J. Ovdi. Tppp/p25 promotes tubulin assemblies and blocks mitotic spindle formation. *Proceedings of the National Academy of Sciences of the United States of America*, 100(24):13976–13981, 2003.

[44] Iva Marija Toli-Nrrelykke, Emilia-Laura Munteanu, Genevieve Thon, Lene Oddershede, and Kirstine Berg-Srensen. Anomalous diffusion in living yeast cells. *Phys. Rev. Lett.*, 93(7):078102–, August 2004.

[45] S. F. Parsons R. Sterba Z. Wang M. P. Sheetz Tran, P. T. and E. D. Salmon. Direct measurement of microtubule flexural rigidity with the laser trap. *Mol. Biol. Cell.*, 6:260a, 1995.

[46] Dejan Trpcevski. Optical stretching of dna as a diagnostic tool in nanotoxicology. Master's thesis, Niels Bohr Institute University of Copenhagen, 2006.

[47] Megan Valentine, Polly Fordyce, and Steven Block. Eg5 steps it up! *Cell Division*, 1(1):31, 2006.

[48] Karen C. Gittes Fred Schmidt Christoph F. van Mameren, Joost Vermeulen. Leveraging single protein polymers to measure flexural rigidity. *The Journal of Physical Chemistry B*, 113:38373844, 2009.

[49] A. C. Maggs M.-F. Carlier Venier, P. and D. Pantaloni. Analysis of microtubule rigidity using hydrodynamic flow and thermal fluctuations. *J. Biol. Chem*, 269:1335313360, 1994.

[50] Lynne Cassimeris Vincent VanBuren and David J. Odde. Mechanochemical model of microtubule structure and self-assembly kinetics. *Biophys J.*, 89(5):2911–2926, 2005.

[51] RA Walker, ET O'Brien, NK Pryer, MF Soboeiro, WA Voter, HP Erickson, and ED Salmon. Dynamic instability of individual microtubules analyzed by video light microscopy: rate constants and transition frequencies. *J. Cell Biol.*, 107(4):1437–1448, 1988.

[52] Gordon H. Orians William K. Purves, David Sadava and H. Craig Heller. *Life: The Science of Biology.* Sinauer Associates, 2000.

[53] Yue Huang Wei Ping Gai Peter C. Blumbergs Peter Hjrup Daniel Otzen Glenda M. Halliday Yun Ju C. Song, Ditte M.S. Lundvig and Poul H. Jensen. p25? relocalizes in oligodendroglia from myelin to cytoplasmic inclusions in multiple system atrophy. *The american journal of Pathology*, 171:1291–1303, 2007.